UNCLASSIFIED

AD NUMBER

AD360459

CLASSIFICATION CHANGES

TO: unclassified

FROM: secret

LIMITATION CHANGES

TO:

Approved for public release, distribution unlimited

FROM:

Distribution authorized to U.S. Gov't. agencies only; Administrative/Operational Use; 11 Jul 1960. Other requests shall be referred to the Defense Atomic Support Agency, Washington, DC 20301. NOFORN.

AUTHORITY

DTRA ltr, 20 Feb 2004; DTRA ltr, 20 Feb 2004

THIS PAGE IS UNCLASSIFIED

UNCLASSIFIED

AD NUMBER

AD360459

CLASSIFICATION CHANGES

TO: unclassified

FROM: secret

LIMITATION CHANGES

TO:

Approved for public release, distribution unlimited

FROM:

Notice: Release only to U. S. GovernmentAgencies is authorized. Other certified request-ers shall obtain release approval from DefenseAtomic Support Agency, Washington, D. C. 20301.Release or announcement to foreign governmentsor their nationals is not authorized.

AUTHORITY

DTRA ltr, 20 Feb 2004; DTRA ltr, 20 Feb 2004

Operation

HARDTACK

April-October 1958

Project 6.13

STUDY of VERY-HIGH-ALTITUDE BURSTS
with AIRBORNE UHF RADAR (U)

Issuance Date: July 11, 1960

HEADQUARTERS FIELD COMMAND
DEFENSE ATOMIC SUPPORT AGENCY
SANDIA BASE, ALBUQUERQUE, NEW MEXICO

DDC CONTROL
N052186

GROUP-1
Excluded from autom...
downgrading and declas...

SECRET

Inquiries relative to this report may be made to

Chief, Defense Atomic Support Agency
Washington 25, D. C.

When no longer required, this document may be
destroyed in accordance with applicable security
regulations.

DO NOT RETURN THIS DOCUMENT

SECRET

WT–1659

OPERATION HARDTACK—PROJECT 6.13

STUDY of VERY-HIGH-ALTITUDE BURSTS with AIRBORNE·UHF RADAR (U)

V. L. Lynn, Project Officer
M. A. Herlin
J. S. Clark
W. G. Clay
A. I. Grayzel
J. H. Pannell

Lincoln Laboratory
Massachusetts Institute of Technology
Lexington, Massachusetts

SECRET

FOREWORD

This report presents the final results of one of the projects participating in the military-effect programs of Operation Hardtack. Overall information about this and the other military-effect projects can be obtained from ITR-1660, the "Summary Report of the Commander, Task Unit 3." This technical summary includes: (1) tables listing each detonation with its yield, type, environment, meteorological conditions, etc.; (2) maps showing shot locations; (3) discussion of results by programs; (4) summaries of objectives, procedures, results, etc., for all projects; and (5) a listing of project reports for the military-effect programs.

ABSTRACT

The principal objective of this experiment was to study the backscattering of electromagnetic radiation caused by products of high-altitude nuclear detonations in the UHF radar band. Two airborne radars were instrumented on frequencies of 425 and 675 Mcps. Several other measurements on propagation effects were undertaken.

The results indicated a pronounced effect which is significant for both scientific and operational considerations. Reflective effects occurred for nearly an hour after the detonation.

Apparent absorption predominated for a period of approximately a minute or less, and was less for the higher burst altitude. This period was followed by one of reflection (or refraction), which lasted in some form for almost an hour. The initial reflections indicated a medium of randomly distributed electron density. Gradually, a shift took place to elongated reflecting regions aligned with the earth's magnetic field, similar in reflective properties to those observed from natural aurora by previous experimenters. The returns of this period were characterized by the following, all observed in polar aurora reflections: (1) altitude of 100 to 150 km; (2) aspect sensitivity, (3) broad spectrum of velocity components, and (4) an apparent east-west motion of the medium.

PREFACE

The data recorded in this report could not have been collected without the wholehearted coop-
eration of the Naval Air Development Unit, South Weymouth, Massachusetts, which assisted
greatly in the actual data collection and also provided flight support and some equipment.

The authors wish to express their appreciation for the advice and assistance of others of
the Lincoln Laboratory staff, especially members of the Radar Division under Jerome
Freedman and the Radio Propagation Group under James H. Chisholm.

We also wish to acknowledge the suggestions and cooperation of Allen Peterson, Raymond
Leadabrand, Rolf Dyce and Lambert Dolphin of the Stanford Research Institute, and of Robert
LeLevier and others of the Rand Corporation.

CONTENTS

7

SECRET

SECRET

SECRET

Chapter 1
INTRODUCTION

1.1 OBJECTIVES

The general objective of this project was to study the effect of a very-high-altitude, megaton-range nuclear detonation on electromagnetic radiation, primarily in the ultra-high-frequency (UHF) radar band. This purpose was to be fulfilled by the following specific objectives, which are presented roughly in order of priority:

(1) Quantitative measurement of the scattering cross section of the ionized cloud at radar frequencies of 425, 675 and 9,375 Mcps.

(2) Quantitative measurement of the geographical extent of radar return from the cloud at the same three radar frequencies.

(3) Measurement of the Doppler spectrum of radar return from the ionized cloud at radar frequencies of 425 and 675 Mcps.

(4) Measurement of the change in thermal noise in passive systems at frequencies of 32, 113, 425, 450 and 675 Mcps.

(5) Measurement of the attenuation due to the ionized cloud on frequencies of 225, 450, 1,500 and 2,900 Mcps.

1.2 PRESENTATION OF THE EXPERIMENTS AND RESULTS

This report deals principally with the experiments at 425 and 675 Mcps since these provided the bulk of the information and since these data are of prime interest. The results of the radar experiment at 9,375 Mcps and the passive experiments (objectives (4) and (5) of paragraph 1.1) are mentioned in Chapter 4.

1.3 THEORY AND BACKGROUND

A nuclear burst in the upper atmosphere produces, even outside the thermally excited volume, high concentrations of electrons, the distribution and duration of which will depend on the actual burst height. Early estimates based on the expected effect of nuclear weapons on the upper atmosphere indicated that effects significant to the propagation and scattering of radio-frequency (RF) energy can thereby be produced over areas of thousands of square miles and can last for several hours.

Previous studies by numerous workers (Reference 1) showed that the most important effect is the production of a heavily ionized stratum by radiation from the burst. For Shot Teak (76 km altitude), it was predicted that this stratum would have a lower boundary at about a 30-km altitude and would have a radius, for an initial electron concentration of greater than $10^6/$ cm^3, of 100 to 500 km (Reference 2). The electron density rises steeply at shorter radii, not only because of the inverse-square-law effect, but also because of the heavy ionization produced by soft x-rays that constitute a large fraction of the total energy released.

Although high electron densities are produced by nuclear bursts in the lower atmosphere, their effects are mitigated by the smaller volumes involved and the higher collision rates; both of these are proportional to atmospheric density, which at 76 km is approximately 10^{-5} times

its value at sea level. At frequencies below 100 Mcps, the dominant effect of low-altitude detonations on RF transmission is strong absorption (Reference 3).

The stratum of dense ionization created by a high-altitude detonation would be expected to diffuse comparatively slowly. Such diffusion would, under the influence of the magnetic field, be ellipsoidal rather than spherical, and would eventually produce a high concentration of ionization centered about the magnetic meridian of the burst.

Radio noise is one of the effects that may be expected if the cloud rises to a height sufficient to permit beta particles to escape from the atmosphere (Reference 4). These beta particles will be trapped in the earth's magnetic field and caused to follow helical paths centered on the lines of force; but some of them will be reflected at high latitudes where these lines converge. Those electrons having relativistic energies will emit a noise spectrum similar to synchrotron radiation with a fundamental frequency of about one Mcps, except that it will be more nearly a continuum. The decay of neutrons emitted from the burst in an upward direction provides another mechanism for producing electrons in this region. The relativistic electrons thus formed can further create ionization over a large area where their paths are such that they reenter the atmosphere.

Thus there are two major effects that are capable of creating large areas of dense ionization which are aligned with the earth's magnetic field. The contributions from either or both of these could produce a condition simulating that of natural auroras.

Strong reflection of RF energy occurs at a point where the frequency of the incident wave is equal to the plasma frequency, approximately $10^4\,N_e^{1/2}$, where N_e is the electron concentration per cubic centimeter. Consequently, a wave of 1,000-Mcps frequency would meet a refractive index of zero at an electron concentration of 10^{10}. It was predicted (Reference 2) that the boundary of the region containing this density would reach a maximum diameter of 60 km. Because of the importance of radar returns from both a scientific and an operational aspect, considerable effort was placed on their detection.

In view of the experimental results, it seems appropriate at this point to discuss some of the theories and results of other experimenters in the study of radar reflections from natural auroras, (Appendix, Figure A.1). The existence of at least two methods of production of field-aligned ionization, by thermal or relativistic electrons, has been noted above.

The properties and causes of the radar reflecting surfaces are not precisely known but a great deal of work has established plausible theories. Booker (Reference 5) argues for the theory that the aurora is associated with columns of ionization lying along the earth's magnetic field, and that echo contributions in different columns combine in more or less random phase. This leads to a requirement of normal incidence of the radar beam with respect to the magnetic lines of force. An example of this loci of perpendicularity is shown in Figure 1.1, and Appendix, Figure A.2. Kaiser, (Reference 6) considering the data and theories of many others, views the reflecting surface as a distribution of relatively dense blobs of ionization which are elongated in the direction of the magnetic lines of force. He regards this as a widespread area of dense, but, on the average, subcritical ionization, in which the electron density fluctuates sufficiently to provide a distribution of over-critical regions. He further shows that the reflecting areas are probably made up of a large number of these scattering elements.

That aspect sensitivity requires essentially specular reflection is widely accepted as a proven experimental fact (References 5, 6, 7, and 9). Not quite so clear is the degree to which the perpendicularity must be met. Echoes have been noted as far as 10 to 14 degrees off the orthogonal condition (Reference 6). Dyce, (Reference 8) observed a large number of auroral echoes at conditions approximately 7 degrees off perpendicularity, operating at 52 Mcps. At 412 Mcps (Reference 9), echoes were observed to approximately 3 degrees off normal incidence. This frequency dependence has been shown (Reference 6) to be fairly well established.

The geometry of the auroral reflection has been delineated by Chapman (Reference 10), and is presented in a simplified fashion in Appendix A of Reference 9. The limits in altitude of the occurrence of returns is commonly accepted as from 90 to 100 km up to 150 to 160 km. Figure 1.1 shows the loci of perpendicularity in slant range and magnetic azimuth for constant

12

SECRET

altitudes of 50, 100, 150 and 200 km for a station near Johnston Island. These curves are based on an effective 11/10 earth's radius to approximate the average index of refraction between the surface and the altitudes of interest.

Beyond this facet of aspect sensitivity, two other characteristics of natural auroras are of interest. The first of these is apparent motion within the aurora. Several experimenters have reported virtual motions of up to 3 km/sec but more usually in the range of hundreds of meters per second. These are commonly observed as fading rates which are roughly proportional to observing frequency. Characteristic values observed are 100 cps at 50 Mcps and 300 to 400 cps at 145 Mcps (References 5 and 6).

The second characteristic of interest in connection with the present experiment is that of frequency dependence of the intensity of the reflected signals. The actual factor of dependence

ELEVATION ANGLES SHOWN BY
DASHED LINES
(represent loci of perpendicularity
at constant elevation angle (ε))
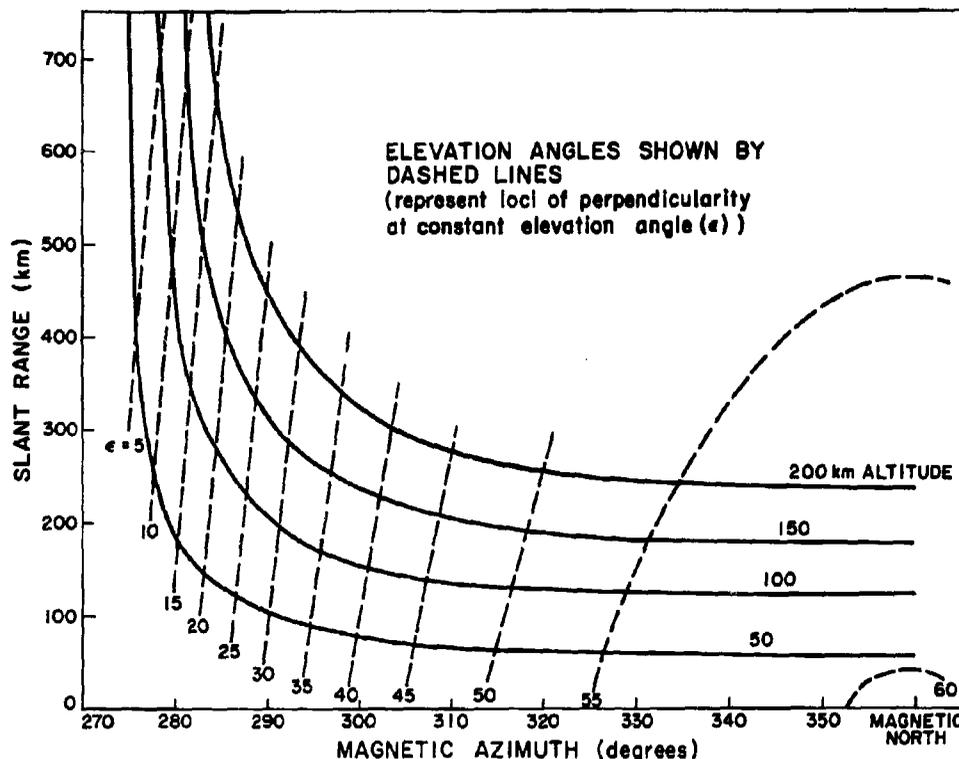
Figure 1.1 Loci of perpendicularity for a station near Johnston Island.

is the subject of some disagreement. However, one auroral display (of approximately an hour's duration) was observed simultaneously on 425- and 675-Mcps ground radars at Round Hill, Massachusetts. The beamwidths used were, respectively, 2.5 and 1.8 degrees. The ratio in the power received was approximately 6.5, 425 Mcps being of greater intensity.

Non-deviative absorption occurs when the collision rate is sufficiently high, as it is at sea level, while refractive effects are predominant when this rate is low. By passive tracking of rocket-borne transmitters or by radar tracking of missiles and of chaff, it would be possible to obtain information to determine which effect prevails, to what extent, and at what altitude.

Attenuation was expected to predominate at early times on all frequencies during the Teak shot. Although quantitative predictions were subject to large uncertainties, they may indicate

SECRET

the order of magnitude of the expected effect. Latter and LeLevier, of the Rand Corporation, suggested that the two-way attenuation occurring on a vertical path at a horizontal distance of 100 km from air zero, at H plus one minute, would be 6 db at 1,000 Mcps and 300 db at 100 Mcps. (This prediction was revised sharply downward shortly before these tests when new electron-attachment-rate data were available.)

The effects of very-high-altitude bursts on radar and communications systems are of the utmost significance to military operations, particularly in missile defense. Radar blinding by persistent absorption or clutter effects could readily be employed by the offensive side to deny radar information to the defense. Even if such effects are not persistent, they may seriously hamper the employment of high-yield nuclear weapons in the defense system. Again, small but unknown amounts of refraction of the radar beam may lead to intolerable errors in the trajectory prediction. The possibility of producing radio noise is a matter of such gravity that its implications are well understood (References 4 and 11).

SECRET

Chapter 2
PROCEDURE

2.1 DESCRIPTION OF THE RADARS

The 425- and 675-Mcps radars were installed in two Navy WV-2 Super Constellation aircraft from the Naval Air Development Unit at South Weymouth (Figure 2.1). The antenna in each case was mounted in the lower radome and continuously rotated in azimuth.

The operating parameters of the two radar systems are shown in Table 2.1. In general, the performances of the two systems are comparable, considering the free-space gain patterns. However, with the antenna mounted below the aircraft fuselage, the vertical patterns are distorted and deflected somewhat downward by the structure. The magnitude and shape of the pattern is thus dependent on the azimuth with respect to the aircraft heading (relative azimuth). These variations have been measured by scale-model studies and are available (References 12 and 13).

The 425-Mcps antenna used was a 14-dipole horizontal array with parabolic (vertical-plane) reflector. It was built by the Naval Research Laboratory and is described in Reference 12. The 675-Mcps antenna, built by the National Research Council of Canada, was a horn-fed pill-box (Reference 13). Both were rotated at approximately 6 rpm. These antennas, with wide vertical patterns (apertures about 17 × 4 feet), were not steerable in the vertical plane.

The transmitters used were similar versions of the AN/APS-70 experimental series. At 425 Mcps, the XD-3 model equipment was operated with a QK-508 magnetron. At 675 Mcps, a modified SC-1 model transmitter utilized a QK-517 magnetron.

The receivers were essentially identical, with the exception of the frequency of the RF amplifier and first stable local oscillator (stalo). A functional block diagram of the receiver, in the configuration used, is shown in Figure 2.2. Detailed descriptions of the operation and theory of this receiver can be found in References 14 and 15, respectively.

The noise-monitor output was used to monitor the noise level, and is described in Chapter 4. The other four video outputs are of interest in consideration of the radar data. The logarithmic (Log video) and linear (Lin video) videos are basically derived by nothing more than a simple, double-conversion receiver, having respective characteristics of response as evident. All the basic data (as to amplitude and location of the returns) were obtained by combinations of these two videos.

The remaining circuitry forms the intermediate-frequency, time-averaged, clutter-coherent, airborne radar (IF-TACCAR) system. This system produces a phase representation of observed signals with corrections applied to eliminate radar-platform motion. Its normal output is the airborne-moving-target indication (AMTI) video which discriminates against targets with no (or little) motion over the earth's surface. It further discriminates against velocities that are integral multiples of 207 knots. Thus, because of the phase repetition, there would be ambiguities of velocity beyond this range.

The bipolar video is a presentation of the pulse-to-pulse phase comparison. It was used to determine coherency of the returns and could be utilized to determine the velocity spectrum.

2.2 DATA RECORDING

Linear and logarithmic videos were displayed on amplitude-time (A-scan) oscilloscopes and photographed with 16-mm Cine-Kodak Special II cameras operating at speeds of 6 to 50

15

SECRET

Figure 2.1 Photograph of Navy WV-2 Aircraft.

frames per second. During this time, the antenna was rotating at approximately 6 rpm.
Therefore, the sector of interest appears for only a fraction of the 10-second cycle. The
sweep widths included the full interpulse period.

Plan-position indicator (PPI) displays of both AMTI and linear video were photographed
scan-by-scan with Fairchild Model 0-15 recording cameras. For each antenna rotation,
a time-exposure photograph of the entire scan was made. This was primarily used as a check
on the basic data recording described above. In addition to this, an observer monitored one
PPI display during the operation, recording pertinent comments regarding the effects.

TABLE 2.1 RADAR PARAMETERS

	Frequency, Mcps	
	425	675
Peak Power (Mw)	2.0	1.2
Average Power (kw)	3.6	2.2
Repetition Rate (cps)	300	300
Pulsewidth (μsec)	6	6
Noise Figure (db)	5	6.5
Bandwidth (kcps)	180	180
Minimum Discernible Signal (−dbm)*	117	114.5
Free-Space Antenna Gain (db)	19	23
Horizontal HPBW (deg)	9.5	6
Polarization	Horizontal	Horizontal

*−dbm = decibels below one milliwatt.

A two-gun (dual-beam) oscilloscope (Tektronix Model 551) was used to display simultaneous
sweeps of bipolar and logarithmic videos. The latter was used only as an identifying device
for signals on the bipolar video. The sweep length of this scope was approximately 100 μsec,
with the origin of the sweep variable in range. An observer attempted to set this range in such
manner that the sweep was centered in the area of returns.

This scope was then photographed with a "streak" camera (high-speed film transport, no
shutter) to obtain pulse-to-pulse pictures of the returns. As the antenna scanned, the camera
was operated in bursts, started just before the area of returns was scanned, and stopped when

16

SECRET

TRANSMITTER PULSE

RF 60Mcps

RF FROM DUPLEXER

RF GROUNDED-GRID AMPLIFIER

CRYSTAL MIXER

FIRST STALO

MIXER

60-Mcps AMPLIFIER

60-Mcps AMPLIFIER

BANDWIDTHS AT 60Mcps WERE 4 Mcps

60-Mcps AMPLIFIER

60-Mcps AMPLIFIER

MIXER

9-Mcps NARROW-BAND AMPLIFIER

MIXER

TUNABLE PHASE-LOCKED STALO

MIXER

51Mcps

51-Mcps AMPLIFIER

LOGARITHMIC AMPLIFIER AND DETECTOR

9-Mcps NARROW-BAND AMPLIFIER

LOG VIDEO

LIN VIDEO

LINEAR AMPLIFIER AND DETECTOR

LINEAR AMPLIFIER DETECTOR AND INTEGRATOR

9-Mcps- VOLTAGE-TUNED OSCILLATOR

NOISE MONITOR

LIMITING AMPLIFIER

3333-µsec DELAY LINE

LINE DRIVER (amplifier)

BOXCAR CIRCUIT

VARIABLE DELAY

AMPLIFIER

OBSERVING PHASE DETECTOR

CORRECTING PHASE DETECTOR

SAMPLING RANGE GATE

AMTI VIDEO

BIPOLAR VIDEO

Figure 2.2 Functional block diagram of radar receivers.

17

it had been passed. No data were obtained except at 425 Mcps on the Orange shot.

Time and antenna-azimuth correlation information were recorded on a multichannel, paper-stylus recorder (Brush Model 208). The time base was a 1-cps square wave generated by a motor-driven cam, which was recorded along with references to world time and burst time and operated Veeder-Root counters which were visible on all photographically recorded data. Antenna-azimuth information was recorded against this time base in the form of a cam-driven pulse appearing on every scan at a fixed azimuth.

An audio, magnetic-tape recorder was wired into the aircraft intercommunication system so that observers at several stations could record pertinent remarks.
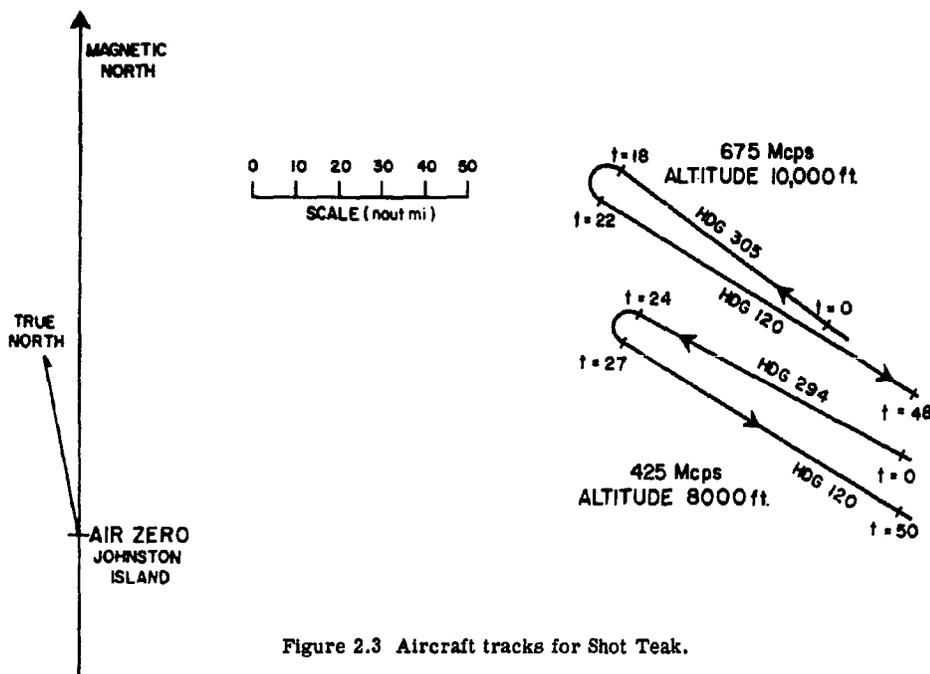
Figure 2.3 Aircraft tracks for Shot Teak.

2.3 FLIGHT OPERATIONS

Figures 2.3 and 2.4 show the positions of the aircraft during the tests. The aircraft arrived on station at least one hour prior to scheduled burst time and remained at least 30 minutes after the last useful observations. They were based at the Barber's Point Naval Air Station at Oahu, T.H.

2.4 BASIC DATA REDUCTION

The major effort in the data reduction was the transferring of signal-intensity and location information from the film recordings to a more usable form. After considering means of presentation, a contoured PPI-type of representation was chosen; this comprises a family of constant-amplitude, contour curves drawn in the geographic plane.

To obtain these curves, each frame of the 16-mm A-scope film was tabulated with range as a function of 5-db signal-increment levels. The frame was assigned the center bearing of that frame, determined as described below, and the points for each signal amplitude were plotted on a geographic plot and connected. This method leads to inaccuracies, the magnitude

18

of which are dependent on the camera speeds used in photographing the displays. It is hoped that these inaccuracies average out over a large statistical sample. Figure 2.5 demonstrates the sources of the error. Figure 2.5(a) shows the photography as a function of exposure and film change over a sector of antenna rotation; (b) indicates the actual contours possible which would be represented in the data-reduction process by the plots in (c); and (d) shows the arbitrary method by which the plots were connected.

After each plot was completed and connected, the result was compared with the PPI photograph of the same antenna scan. By observing this more-integrated display, it was possible to discriminate against ship and aircraft targets, and interference bursts, which might have been chosen from the A-scope. The contours were also checked, by this editing process, for consistency with the actual returns. (During this operation, it was decided that the lowest-
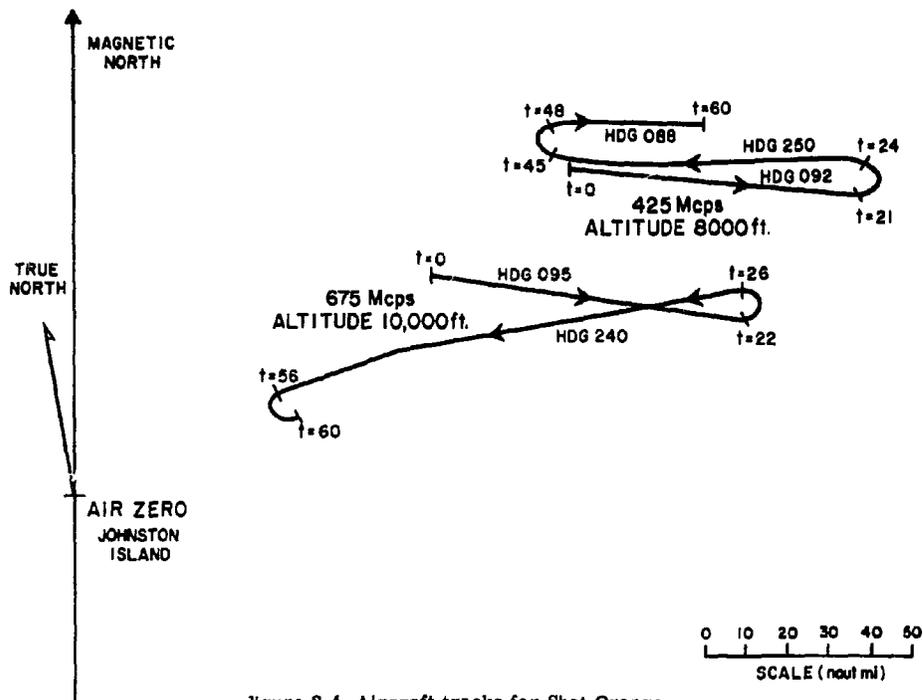
Figure 2.4 Aircraft tracks for Shot Orange.

intensity contour should not be included. Thus all signals from noise to 5 db above noise were discarded. This was felt necessary because of the gross inaccuracies in determining the point in range at which the signal appeared above the receiver noise on an A-scan. The contours indicating the emergence of signals from noise were so far out of agreement with the PPI presentations that they were considered useless.) The range information for remaining contours is considered accurate to within approximately 2 miles.

The azimuth of the center bearing for each frame was determined by a somewhat less accurate method. The camera-drive motors were considered to run at a constant speed over a 10-second period. This appears to be a reasonable, but not precise, assumption. The azimuth from a reference point on a given frame was determined by dividing one scan (360 degrees) by the number of frames occurring over that rotation and multiplying by the number of frames preceding it.

19

SECRET
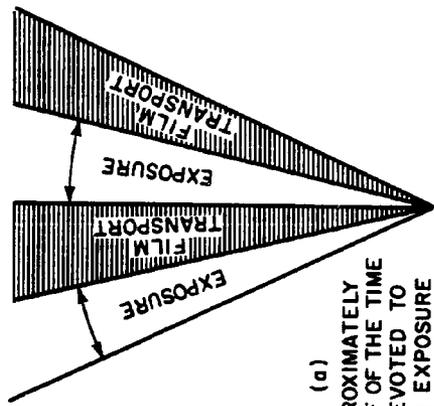
(a)

APPROXIMATELY HALF OF THE TIME IS DEVOTED TO FILM EXPOSURE
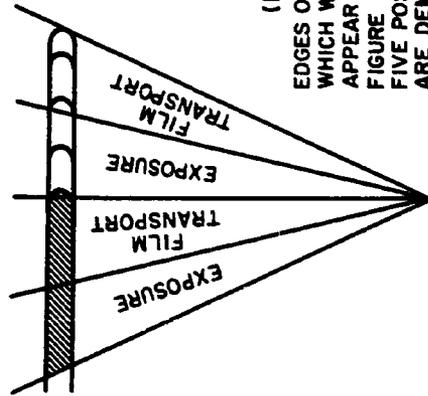
(b)

EDGES OF SIGNALS WHICH WOULD ALL APPEAR AS IN FIGURE 2.5(c). FIVE POSSIBILITIES ARE DEMONSTRATED
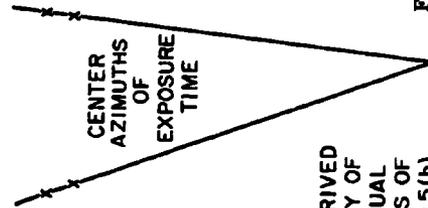
(c)

PLOT DERIVED FROM ANY OF THE ACTUAL CONTOURS OF FIGURE 2.5(b)
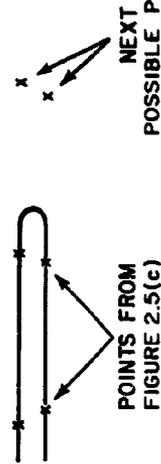
(d)

METHOD BY WHICH PLOTS OF FIGURE 2.5(c) WERE CONNECTED

Figure 2.5 Sources of errors in plotting azimuths.
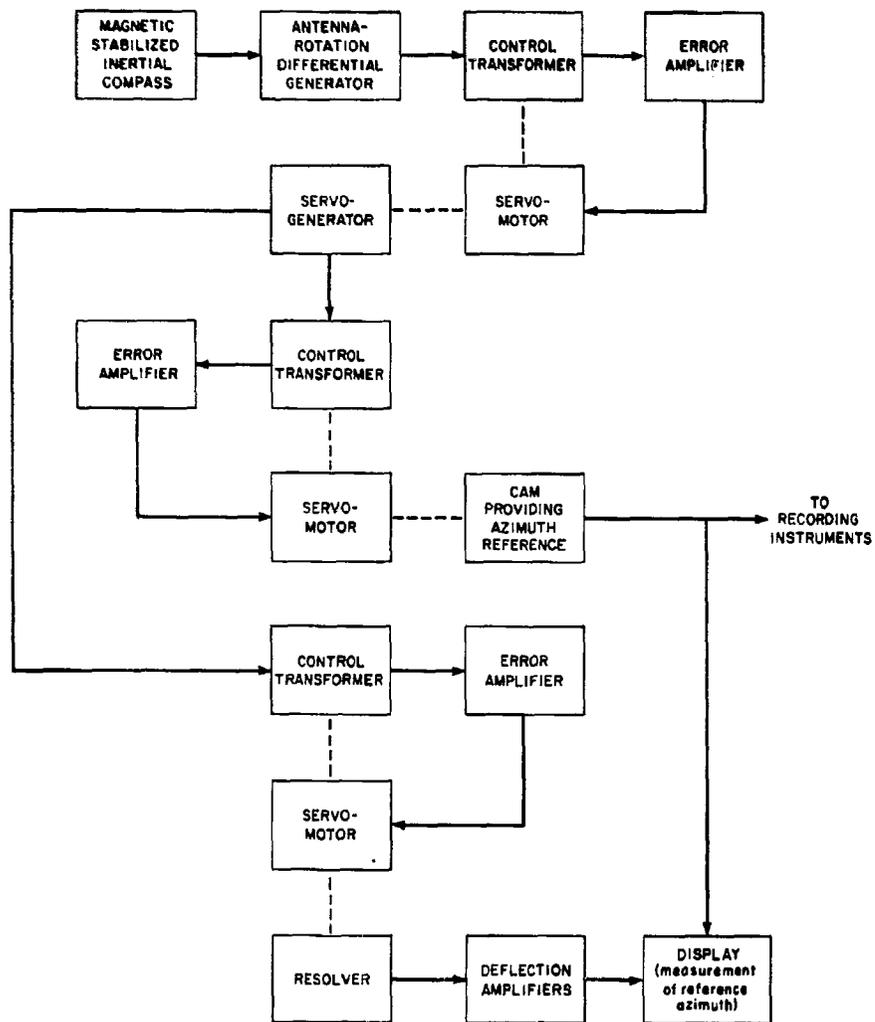
Figure 2.6 Block diagram of servo-system providing azimuth reference.

The azimuth at the reference point was assumed to be a constant magnetic azimuth but this, again, was subject to fluctuations. A diagram of the circuit for determining this reference azimuth is shown in Figure 2.6.

The possible contributions to azimuthal error in the reduced data are summarized as follows:

(1) Constant error (possibly as much as 5 or 6 degrees) in magnetic azimuth of reference point in scan.

(2) Variable error in determination of the azimuth assigned to a given frame, through variations in camera-drive speeds or antenna-rotation speeds.

(3) Variable error in connection of plotted points. This inaccuracy can be fairly large since, in some cases, the distance between frame centers is as great as 6 degrees.

SECRET

Chapter 3
RESULTS

3.1 INTRODUCTION

Data were obtained on 425- and 675-Mcps radars on both the Teak and Orange shots. Figure 3.1 is a summary of the data available for study and is in the form of a three-level histogram plotted against time after burst. The upper two levels indicate times of observation distinguished only by whether or not signals were detected. The third level indicates periods during which, for various reasons, no observations were made. Thus, the shaded areas of level 1 represent the usable data.

It is clear from Figure 3.1 that the most-continuous data were obtained on the lower frequency on the Orange shot, during the time from detonation to approximately 27 minutes later. For this reason, this interval of data was principally considered in the analysis, all others being compared with it.

3.1.1 Data Presentation and Availability.
The most condensed form of the data, which retains essentially all the available information, is represented by a drawing for each scan of the antenna. These drawings show the signal-strength contours in 5-db steps on a geographic plane with a scale of 20 miles per inch. (Since the drawings are in color, the contours are readily distinguished. The complete set of color drawings is available through Chief, Defense Atomic Support Agency, Washington 25, D.C.) All the returns appeared to the west of the radar platform and most are in the northwest quadrant. Thus, this presentation can be thought of as an expanded portion of the PPI scope, encompassing only the west sector beyond 50 to 100 miles. Symbols indicate the geographic locations of air zero and the radar platform and also the direction of magnetic north. Sample presentations of the same information in black and white on a reduced scale are shown in Figures 3.2 to 3.11.

3.1.2 Objectives of the Analysis.
The data were analyzed with several objectives. The main objective was the achievement of a clear understanding of phenomena free from distortions of measurement techniques (e.g., the distinction between antenna gain pattern and true frequency dependence).

Other objectives included the determination of radar-frequency dependence, burst-altitude dependence, auroral similarity, and post-burst-time dependence.

3.2 QUALITATIVE DESCRIPTION OF BACKSCATTER SIGNALS

3.2.1 425-Mcps, Shot Orange.
Signals were detected on almost every scan of the antenna (approximately every 10 seconds) from H + 1 minute to approximately H + 21 minutes when the aircraft turned. Thus a fairly clear picture of the backscatter evolution can be seen. The stages of this growth overlap, but can be roughly divided into four phases: (1) a period when no return was observed; (2) a period when returns were closely confined to the space near air zero; (3) a period when expansion and apparent north-south elongation occurred; and (4) a period when only the northern extremes of the Phase 3 returns remained, and an apparent east-west elongation occurred. The times after burst corresponding to these phases were approximately as follows:

Phase 1	0 to 1 minute	Phase 3	3 to 6 minutes
Phase 2	1 to 5 minutes	Phase 4	6 minutes to last observed signals

23

SECRET

Examples of the signals observed are shown in Figures 3.2 to 3.11. In these drawings, the signal strengths are given in decibels below one milliwatt (–dbm); the location of air zero is shown by a cross, with magnetic north indicated by a line connecting this cross and the vertical arrow. The location of the radar station is off the drawing to the right but designated by an arrowed-circle at a point 100 nautical miles to the west of the station. It should be noted that the location of air zero is given in horizontal range while the returns are plotted in slant range. Thus, a return from an altitude of 100 km at a distance of 150 naut mi, which is directly over air zero at a given time, will be shown at a range of 9 miles beyond air zero.

The first signals observed (H + 1.0 minutes) are shown in Figure 3.2 and are characteristic of Phase 2. Figure 3.3 shows the next scan of the antenna at H + 1.13 minutes. The signals remained very intense and concentrated about air zero until about H + 2.5 minutes, when they disappeared for two scans and then returned. At about this time, the characteristics of
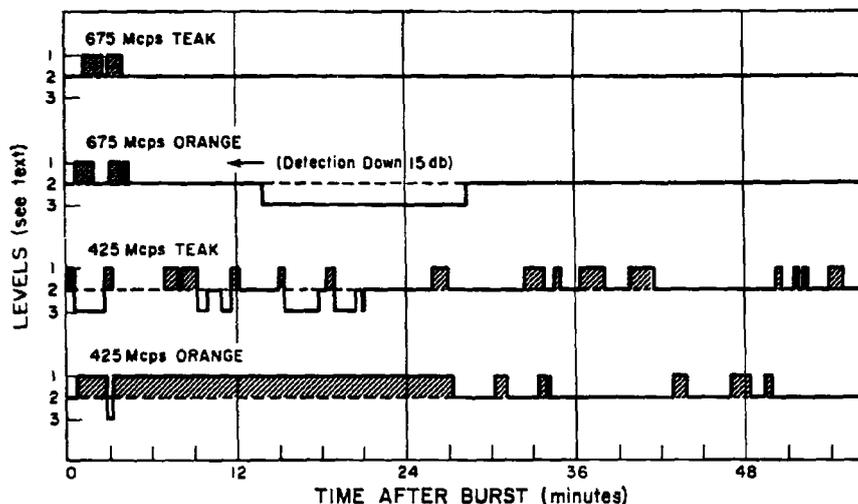
Figure 3.1 Histogram summary of data available for study.

Phase 3 were observed as shown in Figure 3.4 with the Phase 2 returns still present. At H + 3.35 minutes (Figure 3.5), both phases are still present, but both have intensified and elongated. At H + 4.53 minutes (Figure 3.6), the north-south elongation of Phase 3 had continued, giving rise to an apparent northerly motion. The Phase 2 return still present was followed by a similar but weaker signal on the next scan and thereafter disappeared. At H + 5.13 minutes (Figure 3.7), the Phase 3 returns had reached the northern limits to which they were observed, and at H + 6.03 minutes (Figure 3.8), the last apparent northern motion is accompanied by the commencement of east-west elongation (Phase 4). Figures 3.9 to 3.11 show further returns in Phase 4. All signals occurring after H + 6 minutes were found in approximately the area covered by these three examples and, until H + 21 minutes they retained approximately the same size and intensity.

At approximately H - 21 minutes, the aircraft turned about 180 degrees. During the turn, the signals intensified momentarily and then disappeared, reappearing sporadically until H + 50 minutes when the last returns were observed. At about H + 47 minutes, the aircraft again reversed course and the signals again intensified during the turn.

The appearance of the returns on an A-scan presentation (range versus amplitude) resembled that of land returns, being spiked and much less homogeneous than those occurring from ocean-surface or storm-weather backscatter.

24

SECRET
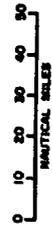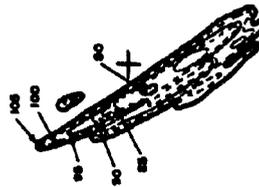
Figure 3.3 Returns, 425 Mcps, Shot Orange,
H + 1.13 minutes.

NAUTICAL MILES
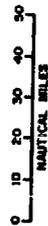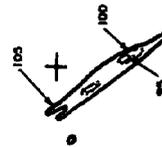
Figure 3.2 Returns, 425 Mcps, Shot Orange,
H + 1.0 minutes.

NAUTICAL MILES

Figure 3.5 Returns, 425 Mcps, Shot Orange, H + 3.35 minutes.

Figure 3.4 Returns, 425 Mcps, Shot Orange, H + 2.90 minutes.

26

SECRET

Figure 3.7 Returns, 425 Mcps, Shot Orange, H + 5.13 minutes.

Figure 3.6 Returns, 425 Mcps, Shot Orange, H + 4.53 minutes.

27

SECRET

Figure 3.9 Returns, 425 Mcps, Shot Orange, H + 6.76 minutes.

Figure 3.8 Returns, 425 Mcps, Shot Orange, H + 6.03 minutes.

28

SECRET

Figure 3.11 Returns, 425 Mcps, Shot Orange,
H + 18.93 minutes.

Figure 3.10 Returns, 425 Mcps, Shot Orange,
H + 7.97 minutes.

29

SECRET

3.2.2 425-Mcps, Shot Teak. On Shot Teak, there is some doubt as to the accuracy of the locations given for air zero. Those used represent the best compromise between facts and reasonable assumptions. Thus the qualitative description of the evolution of the returns with respect to the location of air zero is based on less than positive knowledge. In general, however, it is safe to state that the growth is similar to that described in Paragraph 3.2.1 above, although signals were considerably less intense and less spread.

Phase 1 (no returns) was considerably shorter on this shot, and returns near air zero (Phase 2) were observed at H + 0.26 minute, on the second antenna scan after burst. On the following scan, the principal returns appeared beyond air zero and 50 miles to the south, remaining there until H + 2.40 minutes. Phase 3 (north-south elongation) commenced at H + 0.55 minute, and reached its northern extreme (corresponding to the auroral zone for this location) at H + 1.97 minutes. At H + 2.68 minutes, all returns were observed near this northern limit but were not so extensive as those on the Orange shot. The backscatter on any scan seldom exceeded a 10-mile east-west extent. No returns were detected from H + 3.28 minutes to H + 6.96 minutes and, when they reappeared at H + 7.11 minutes, they were located somewhat south of a line magnetic west of the radar location. The signals gradually moved northward until, at H + 9.06 minutes, they were reoccurring in the probable auroral zone and, thereafter, remained in this area.

A major distinction from the characteristics of the Orange shot returns was observed in this later phase. It is not, however, necessarily in disagreement with the results on Shot Orange. Three separate time intervals were characterized by an apparent motion of the reflecting surface in a westerly direction, corresponding to speeds of several hundred meters per second. Since the Shot Orange returns were considerably more spread in the east-west direction, such a phenomenon could have occurred without being detected. In each case, the signals appeared to move westerly until they occurred after the succeeding transmitter pulse, then faded and were later observed again at shorter range. The signals were visible following the next transmitter pulse each time (second-time-around returns), but no analysis could be undertaken because of the presence of sea return.

The first of the apparent westerly shifts was observed from H + 11.30 minutes to H + 17.61 minutes and approximated a velocity of 400 meters per second. At H + 18.66 minutes signals reappeared after a fade and remained until H + 21.20 minutes with no indication of movement. At about H + 26 minutes, returns were observed for one minute, 50 miles west of the previous ones. Five minutes later they again were observed, this time 70 miles to the east, and a second apparent continuous motion to the west took place until about H + 35 minutes. The velocity in this case was approximately 800 meters per second. At about H + 37 minutes, the signals were again observed in motion with an apparent velocity of about 600 meters per second, this time covering a larger area. At H + 40 minutes, the returns appeared over an area which, for the first time, was comparable to that of the first 20 minutes following Shot Orange. This (east-west) extended area then appeared to recede to the limit of long range and faded by H + 42 minutes. Sporadic signals then were observed, with no apparent motion, until the last was detected at H + 54 minutes.

3.2.3 675-Mcps Radar Experiments. Very little data are available with regard to the 675-Mcps radar and a description of their evolution is not possible. They were, therefore, compared with the results on 425 Mcps, Shot Orange, merely to determine the existence of any possible contradictions.

Shot Orange: The detection capability of the system was roughly 15 db lower than that of the 425-Mcps radar because of a receiver malfunction. Under this condition, Phase 1 (no returns) lasted for slightly less than one minute. Signals appeared in the vicinity of air zero for one minute, then faded. Upon their reappearance (H + 3.4 minutes), they gave an indication of north-south elongation but disappeared again at H + 4.5 minutes. No signals were detected for the next 10 minutes and the system was then rendered inoperative while the malfunction was corrected. At approximately H + 28 minutes, the radar was again operating,

30

this time at full sensitivity, and returns were observed for four scans of the antenna. No further signals were detected, although observation continued for more than an hour.

Shot Teak: The radar was operated at full sensitivity (comparable to that of the 425-Mcps radar) and returns were observed as follows: No signals were detected until H + 1.8 minutes, at which time they appeared, already in the auroral zone, well to the north of air zero (approximately 100 miles). The returns remained in this area, confined to less than 5 miles of east-west extent, until H + 4.2 minutes; the returns were observed on all but two of the antenna scans in that period.

3.2.4 Summary. The general form of the appearance of the echoes in location can be summarized as follows:

Phase 1. A short period immediately following the detonation during which no returns were detected from the ionization, and the scopes appeared normal.

Phase 2. A period when the returns appeared in the vicinity of air zero and wore very intense.

Phase 3. A period in which the signals indicate an apparent motion northward and elongate in the north-south direction.

Phase 4. A long period in which all signals are confined to an east-west band, north of magnetic west from the aircraft.

Although the durations of these phases are not clear and they are often concurrent, a rough tabulation can be made, as shown in Table 3.1.

TABLE 3.1   PHASE DURATIONS

Shot	Frequency	Phase (minutes after detonation)			
		1	2	3	4
	Mcps				
Orange	425	0 to 1	1 to 5	3 to 6	6 to 50
Teak	425	0 to $\frac{1}{4}$	$\frac{1}{2}$ to 2	$\frac{1}{2}$ to $2\frac{1}{2}$	2 to 55
Orange	675	0 to 1	1 to $4\frac{1}{2}$	1 to $4\frac{1}{2}$	—
Teak	675	0 to 2	- X -	- X -	2 to 4

The most notable exceptions to the above summary are as follows:
(a) 675-Mcps Shot Teak: No observation of the second or third phases.
(b) 425-Mcps Shot Teak: Occurrence of signals south of magnetic west from H + 7.11 to H + 9.06 minutes.
(c) 425-Mcps Shot Teak: Observation of an apparent motion of the reflecting medium in a westerly direction, with velocities ranging from 400 to 800 meters per second.

3.3   TIME RELATIONSHIP

The determination of the variation of backscattered signals with time was approached in two manners. The first considered the total reflected power on a given scan and the second, the peak signal strength.

3.3.1 Total Reflected Power Versus Time. Figure 3.12 demonstrates the variation of total reflected power with time for the 425-Mcps radar in the 30 minutes following Shot Orange. The representation of power was derived by measuring the area between two adjacent 5-db contours, multiplying by the mean signal strength above noise for that area, and dividing by the range. The latter step compensates for the one-dimensional increase in area with antenna beamwidth. A summation of these relative powers on each antenna scan was then plotted as a function of the time corresponding to that scan. Figure 3.12 shows this function with approximately every fourth scan considered.

31

SECRET

There were insufficient data to warrant such treatment except at 425 Mcps on Shot Orange, during the period shown.

3.3.2 Maximum Signal Strength Versus Time. The second method of presentation is shown in Figure 3.13. This plot, of the most intense signal per scan, disregards all areas of return except that of the greatest intensity. Since there is no consideration of antenna pattern or range in this type plot, it is suitable only for comparison of returns emanating from approximately the same area, such as those during the 6 to 21 minute period shown. While this shows a nearly constant strength over that period, the previous method of display (Figure 3.12) indicated great variation in power returned. Such a difference could be caused by a variation in range.
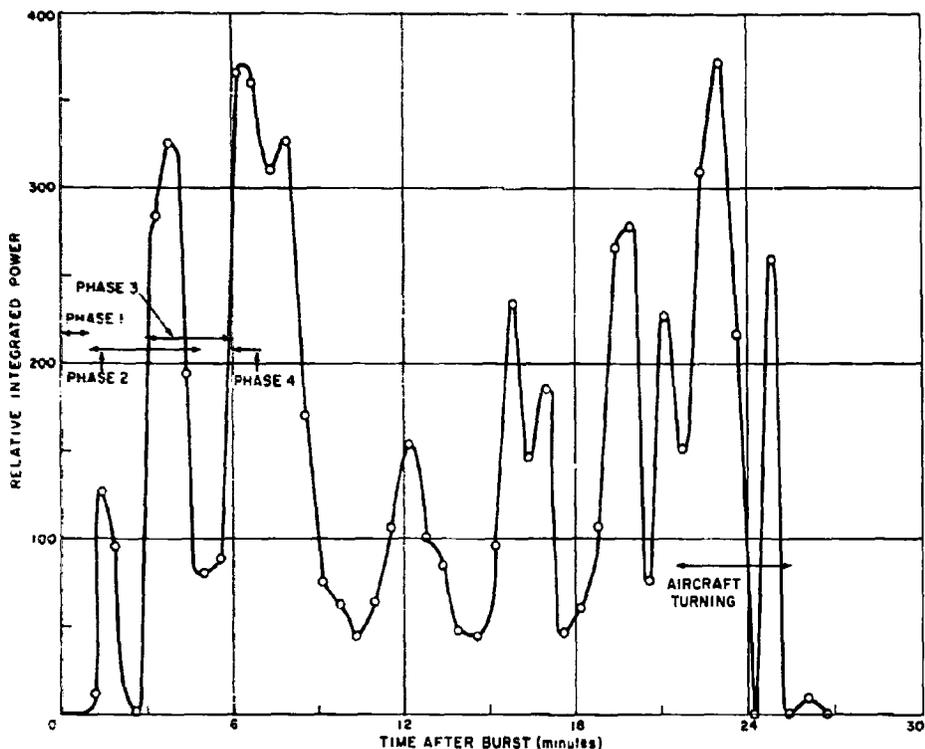
Figure 3.12 425 Mcps, Shot Orange.

3.4 RANGE DEPENDENCE

A rather sharp variation in range was noted on the 425-Mcps Shot Teak data as an apparent motion of the reflecting surface. Although this effect was not observed on Shot Orange, it could have occurred and been masked by the greater extent of returns in the east-west direction, as noted above. As a means of testing this possibility, the period from approximately 6 to 21 minutes was broken into 3-minute intervals. Each blob of return was separately tabulated as to its maximum signal intensity (in db above receiver noise) and the 10-mile range increment within which it occurred. Then, for each three-minute interval, the signal strengths occurring within each range increment were added together. This summation is shown in

22

SECRET

Figure 3.14 for each time interval and represents a distribution of weighted signal strengths as a function of range.

The first time interval (6.33 to 9.30 minutes) does not agree with the others, indicating perhaps that the transition from nonaligned to aligned ionization was still taking place during this time. However, the remaining curves correlate as to occurrence of maxima and minima, and give no indication of any apparent motion of the order of magnitude noted on Shot Teak.

3.5 ANTENNA PATTERNS

The greatest single variable in the data that can be attributed solely to the instrumentation is that of vertical antenna pattern. The influence of the aircraft structure causes this pattern to vary with the azimuth relative to the aircraft heading (relative azimuth). However, if only
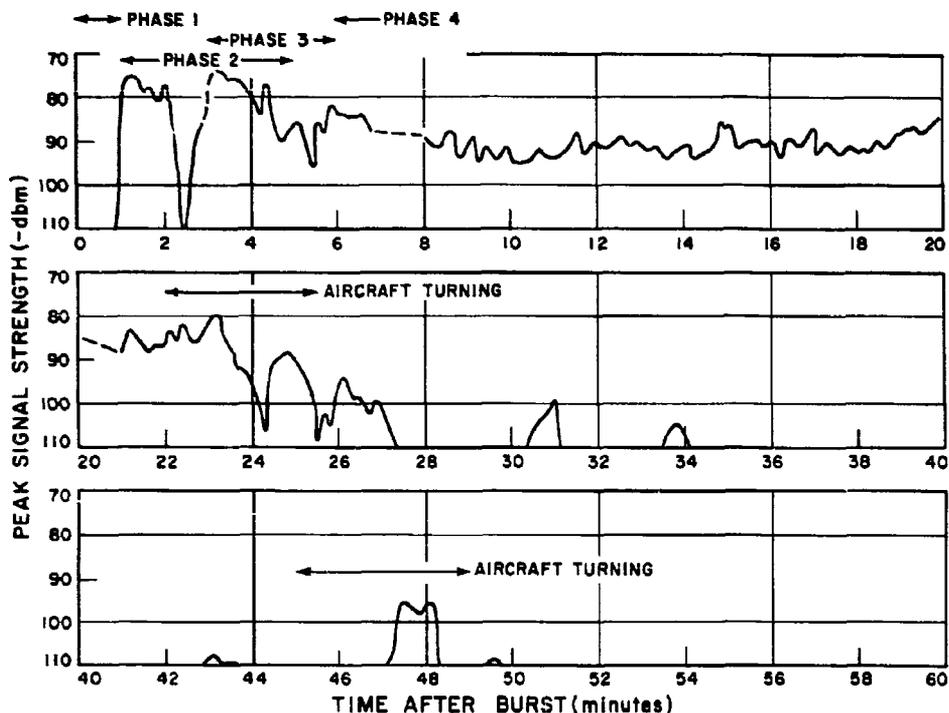
Figure 3.13 Most-intense signal strength versus time, 425 Mcps, Shot Orange.

the field-aligned ionization is considered, the problem of determining the appropriate gain is somewhat simpler. Figure 3.15 shows the curves of Figure 1.1 transferred to a section of a polar plot. If only the condition of orthogonal incidence of the radar beam with the magnetic lines of force is considered, any given range and magnetic bearing from the radar location defines a single altitude, with corresponding elevation angle.

Under these conditions, it is now possible to define the minimum effective cross section that is detectable at any point in space (detection capability). However, in order to do this, the following two assumptions must be made:

(1) Total specular reflection occurs at the ocean surface, that is, the energy is neither absorbed nor scattered. Under sea conditions during the tests, this assumption should lead to optimistic detection capabilities with errors in the 0 to 5 db range, being higher at higher elevation angles. Previous experimental results, Reference 16, indicate magnitudes of 0.2

33

SECRET
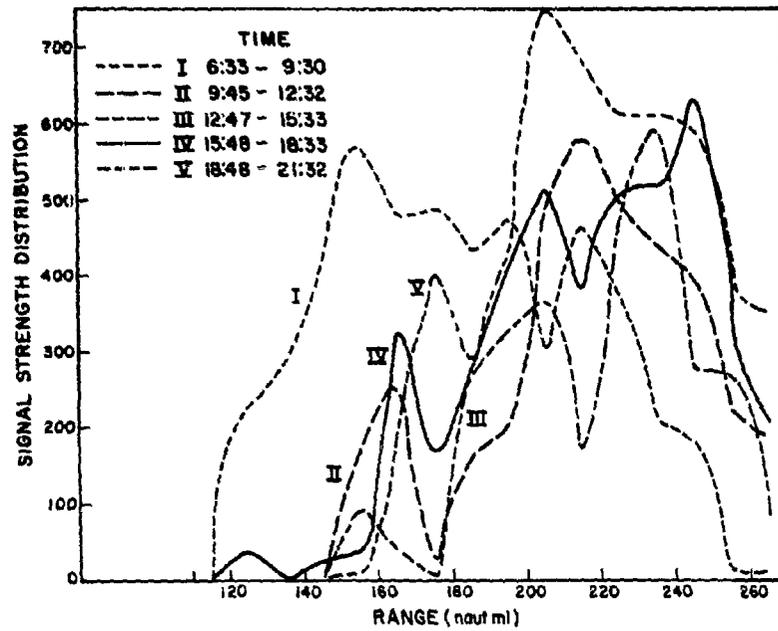
Figure 3.14 Distributions of signal strength in range.
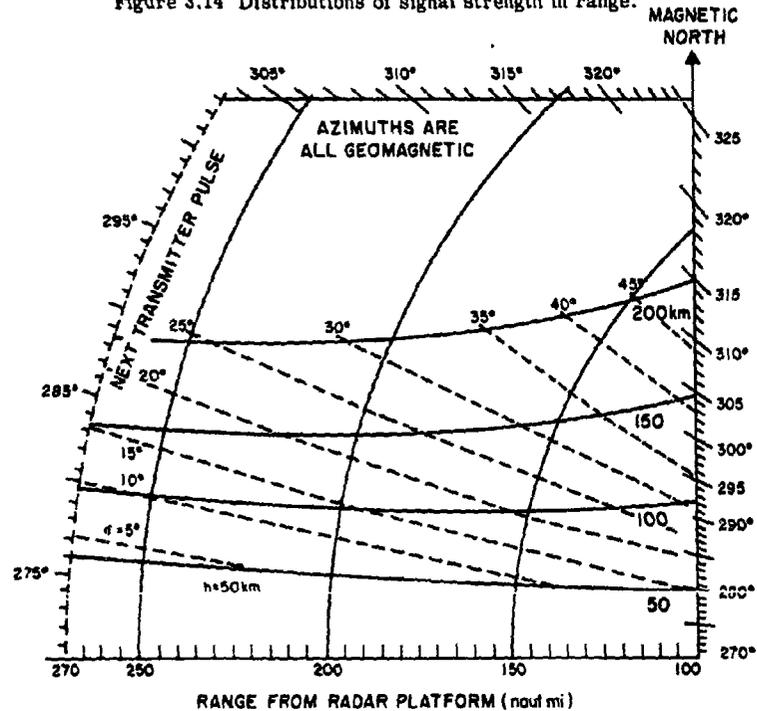
Figure 3.15 Loci of perpendicularity for constant altitude and constant elevation angle.

34

SECRET

to 0.7 db up to 10 degrees elevation (incidence on sea surface), 0.2 to 1.9 db in the 10 to 20 degrees range, and 0.3 to 5.0 db up to 40 degrees.

(2) The backscattering surface does not fill the radar beam in either dimension. This represents a rather arbitrary decision and is further discussed in Paragraph 3.6. It is probable either that this assumption is correct or that the beam is filled in the horizontal dimension only. The possible error introduced is, therefore, represented by the difference between the third and fourth powers of range. In the present analysis, signals lying between 120 and 270 miles were considered, leading to a maximum possible error of 3.5 db. Further, the assumption chosen in this case has an opposite tendency of error from that of the first assumption.

Figures 3.16 and 3.17 depict contours of detection capability for the two radars, subject to the perpendicularity condition, with the aircraft headings used during the early times (approximately zero time to H + 20 minutes) on Shot Orange. Cross sections at altitudes can then be drawn (e.g., Figure 3.24) which take into account the variation of antenna pattern with relative azimuth. These cross-sectional curves are considerably easier to view and only they will be shown in further presentations.

3.6 ALTITUDE OF REFLECTING SURFACE

In each case, the data after the first few minutes exhibit qualities that are similar to the characteristics of radar reflections from natural auroras. It is, therefore, reasonable to assume that these data would also be similar in the less-obvious comparisons. The data of 425 Mcps on Shot Orange, excluding the first six minutes, were used in the treatment described below.

Approximately every sixth scan was considered. Each area of return was examined with regard to the nature of the reflecting surface involved. Only two possibilities were probable: that the reflecting surface at a given range did not fill the radar beam in either dimension and could be approximated by a point target; or that it did fill the beam in the horizontal plane and must be considered as an elongated target. In either case, two other factors tended to smear the returns tangentially.

The E-plane (horizontal) pattern of the antenna (Figure 3.18) contributes in an obvious fashion, and this contribution can be taken into account. There is considerably more speculation involved in the reflecting gain pattern of an area of field-aligned ionization. Chapter 1 referenced previous experimenters (with natural auroras) who had observed backscattering where the radar beam was more than 10 degrees off orthogonal incidence with the magnetic field lines. This effect was also shown to be frequency-sensitive and the indications were that, at the wavelengths used, one should not expect returns unless the perpendicularity condition was satisfied to within about 2 to 3 degrees. It is obvious that, for a given radar frequency, a "gain pattern" of the reflecting surface exists but the actual function is not known.

Each area of return was compared with the E-plane pattern and the resultant unsmeared signal plotted on an overlay. As a matter of convenience, each area was reduced to one dot if such could be reasonably done after consideration of the pattern. In a few cases, it was necessary to draw the reflecting surface as an elongated source. These could be considered, and arbitrarily were, as the summation of contributions from two or three point sources. The resulting overlay is shown in Figure 3.19, an expanded section of a polar geographic plot, and includes the perpendicularity loci for constant altitudes, transferred from Figure 1.1. While the dots cannot be considered to represent the actual scattering areas, they do depict the distribution of locations of returns. Although no corrections could be applied for degree off-perpendicularity, as noted above, the magnitude may be deduced from Figure 3.20, a plot of the boundaries of returns observed at 100-km altitude for incident RF energy up to 5 degrees off orthogonal intersection with the lines of magnetic force.

The plot of Figure 3.19 was then divided into sections 5 miles across, running north and south, and the average location of all dots in each section was found. This is shown in Figure 3.21; the numbers beside the triangular plots show the samples contributing to that

35

SECRET
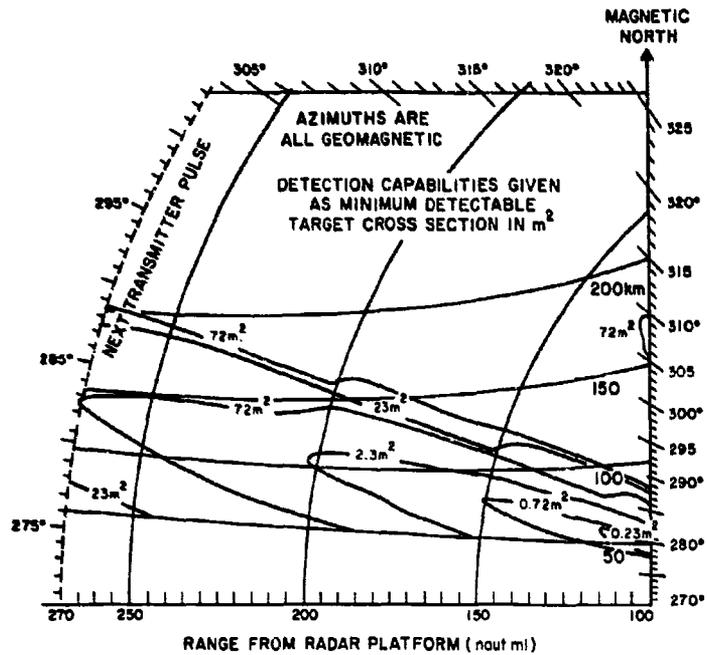
Figure 3.16 Detection capability (orthogonal incidence only) for 425-Mcps radar.
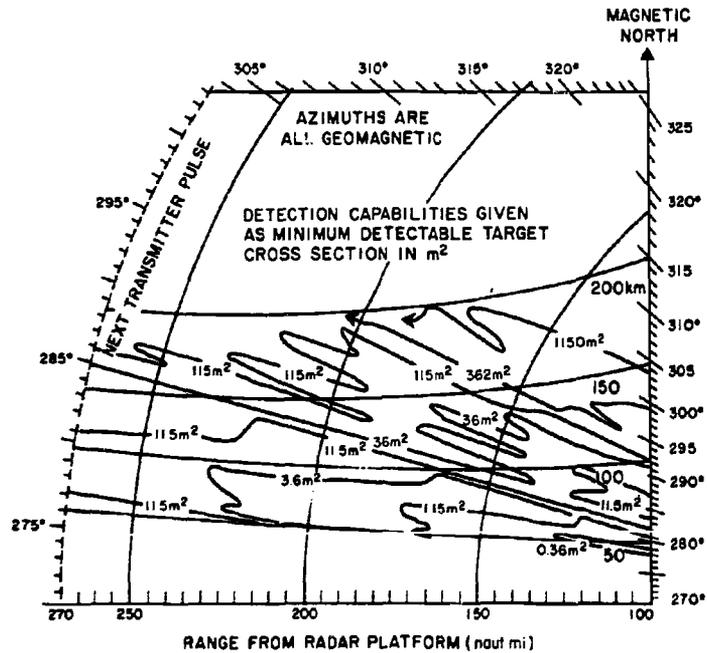
Figure 3.17 Detection capability for 675-Mcps radar.

36

SECRET
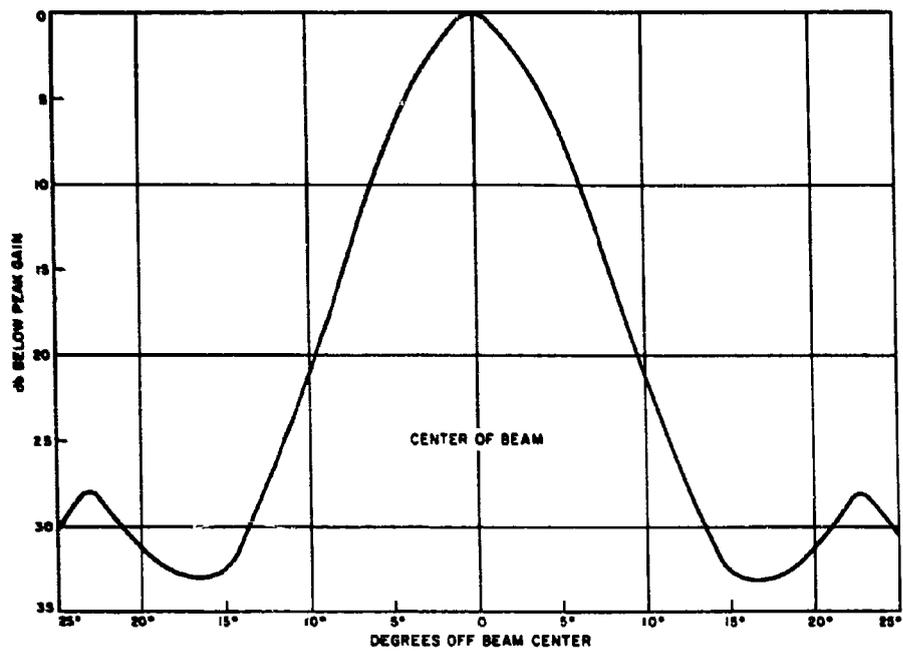
Figure 3.18 425-Mcps E-Plane antenna pattern.
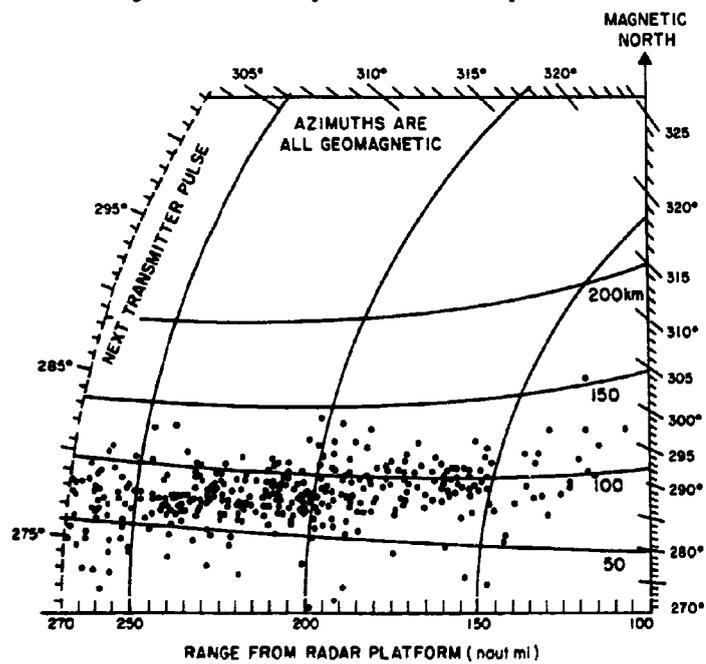
Figure 3.19 Overlay of reflecting surface locations, 425 Mcps, Shot Orange.

37

SECRET
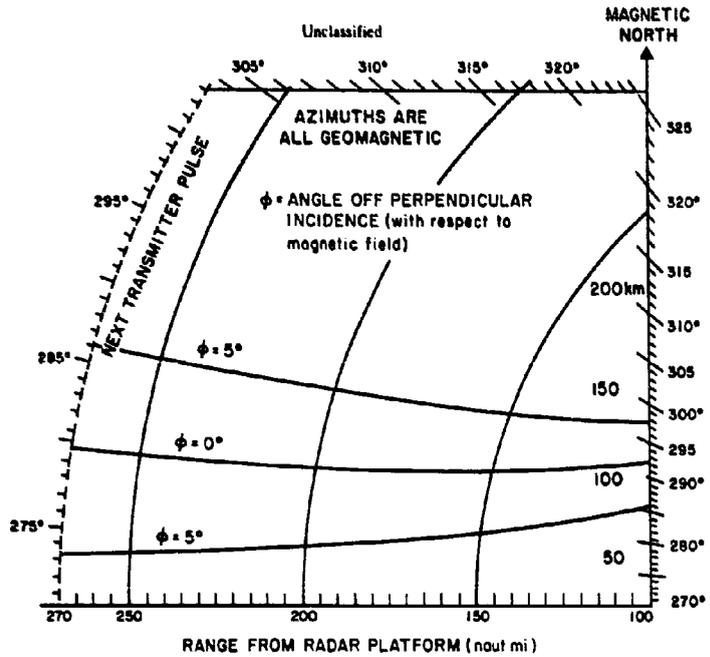
Figure 3.20 Perpendicularity (and 5 degrees off) loci for constant altitude of 100 km.
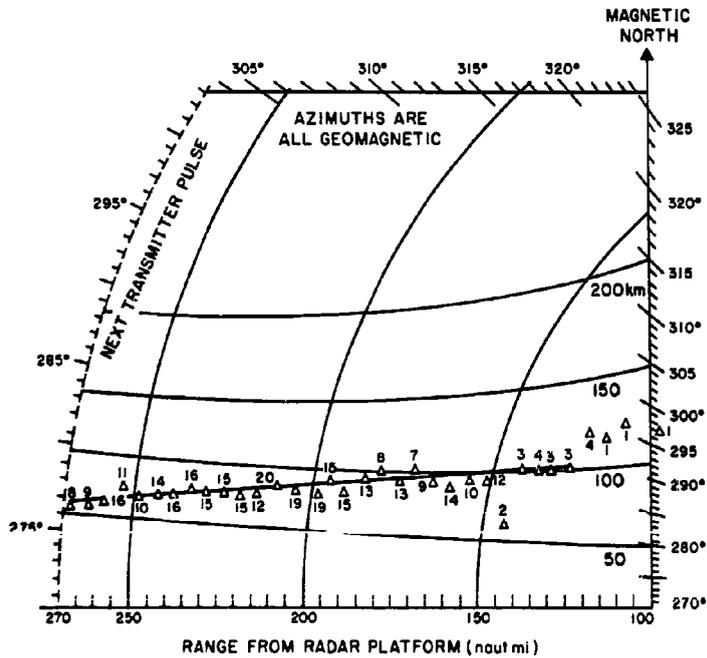
Figure 3.21 Average locations of points plotted in Figure 3.19.

SECRET

average, and hence to its reliability. Thus we can draw a straight line (Figure 3.21) representing the average azimuth-range locations of all returns considered, which fits well for all points except those with few contributing samples.

This line can now be compared with the constant-altitude loci of perpendicularity and is seen to run from the 50-km curve at long range, to the 100-km one at shorter ranges. The possible explanations of height change with range were categorized as follows:

(1) The height change was a real phenomenon. No reasonable explanation was found that would indicate a tendency for the reflecting surface to tilt in this manner.

(2) Erroneous magnetic-field information was used in the calculation of perpendicularity loci. It was felt that this was unlikely in sufficient magnitude to cause the effect.

(3) This effect is a measurement peculiarity due to the antenna pattern. However, since the peak antenna gain occurs at approximately 12 degrees elevation, any tendency to observe the returns, other than at one altitude band, would be expected to have an opposite effect.

(4) This effect is due to a constant error in the azimuths plotted. Such an error could easily be explained (Chapter 2) and is probably most likely.

The last explanation was assumed and, in Figure 3.22, the line representing the average location of returns (from Figure 3.21) has been redrawn and then shifted about the radar location in a clockwise direction, for $4\frac{1}{4}$ degrees. This shift places the line of average location parallel with the perpendicularity loci and at an approximate 125-km altitude.

In Figure 3.23, the positions of the returns (from Figure 3.19) are replotted with an azimuth shift of $4\frac{1}{4}$ F. If we then consider the band of altitude of the reflecting surface as either 100 to 150 km or as 90 to 160 km (either commonly accepted from the radar studies of natural auroras), the following percentages of occurrence are found:

Band, km	Above	In Band	Below
100 to 150	11.5	82	6.5
90 to 160	4	92	4

Only the returns observed on 425 Mcps after Shot Orange were statistically adequate for this treatment in determination of altitude, hence no check was possible using other data. However, a second method, independent of azimuth and magnetic geometry, could be used with the same data.

Since the beam crosses through any altitude plane at an angle of approximately 12 degrees, the range at which maximum gain occurs will be determined by the altitude. Thus, if the average altitude of all reflecting bodies was at 125 km, the probability of detecting a signal of any given amplitude would be greatest at the range that defines the maximum detection capability for altitudes of 125 km (approximately the range at which the center of the vertical-beam pattern passes through that altitude, corrected for inverse fourth power of range). Conversely, if the distribution of signals as a function of range is plotted, then the peak of this curve can be related to an altitude that has its maximum detection capability at that range.

In Figures 3.24 and 3.25, the solid curves represent the detection capability of the 425-Mcps radar after Shot Orange. The dotted curves represent the actual observed distribution of signals in range. This distribution, shown in Figure 3.24, was derived by taking the summation of peak signal strengths occurring in each 10-mile increment during the 6 to 21 minute period following Shot Orange. Thus it is merely the summation of the curves shown in Figure 3.14. In Figure 3.25, the distribution represents the percentage of the total reflected power occurring in each 20-mile increment, the power being obtained as described in Paragraph 3.3.1.

These two presentations are similar and merely represent two methods of approach. Both can clearly be seen to achieve maximum value between the 100- and 150-km curves, thus confirming the previous altitude determination.

39

MAGNETIC
NORTH

AZIMUTHS ARE
ALL GEOMAGNETIC

305°
310°
315°
320°
325
320°
315
200km
310°
285°
AFTER 4-1/4 DEGREES OF ROTATION
ABOUT THE RADAR STATION
305
150
300°
295
275°
100
290°
AS TRANSFERRED
FROM FIG. 4.21
280°
50
270°
270   250   200   150   100

RANGE FROM RADAR PLATFORM (naut mi)
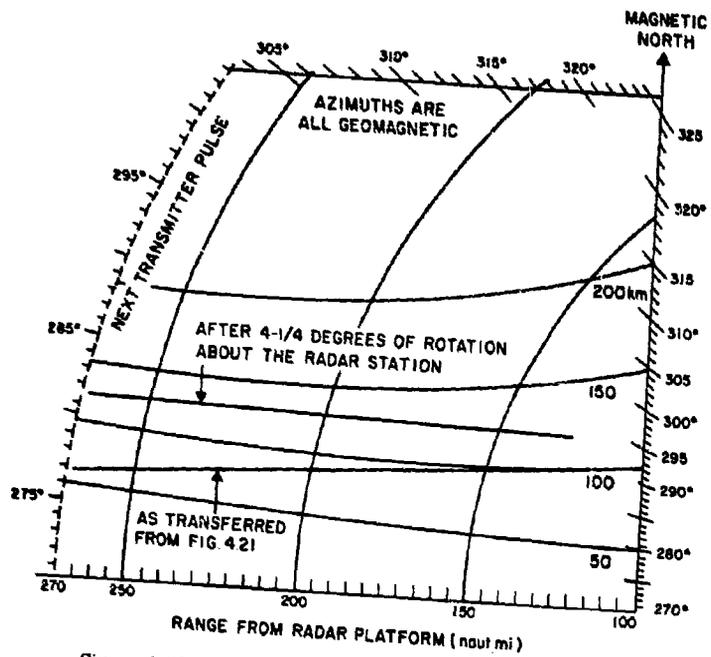
Figure 3.22 Average locations of returns considered.

MAGNETIC
NORTH

AZIMUTHS ARE
ALL GEOMAGNETIC

305°
310°
315°
320°
325
320°
315
200km
310°
285°
305
150
300°
295
275°
100
290°
280°
50
270°
270   250   200   150   100

RANGE FROM RADAR PLATFORM (naut mi)
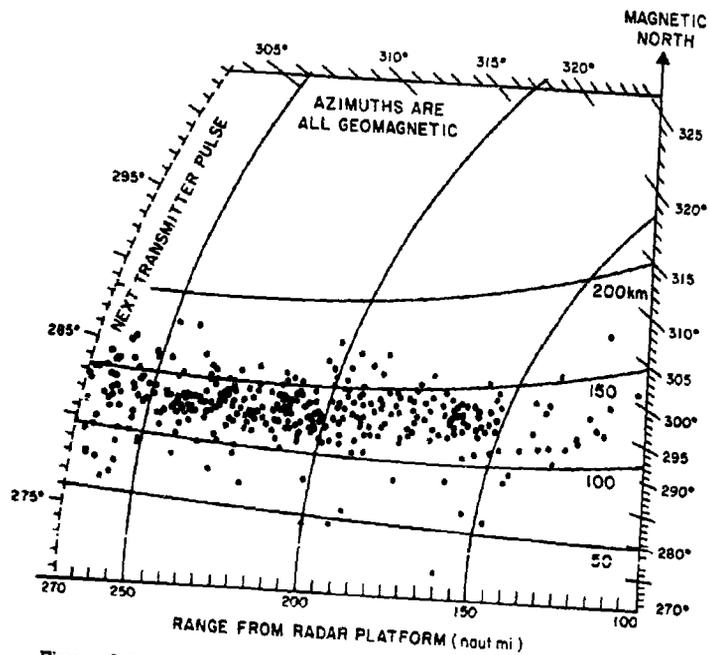
Figure 3.23 Return distribution after 4¼ degree azimuth shift.

40

SECRET
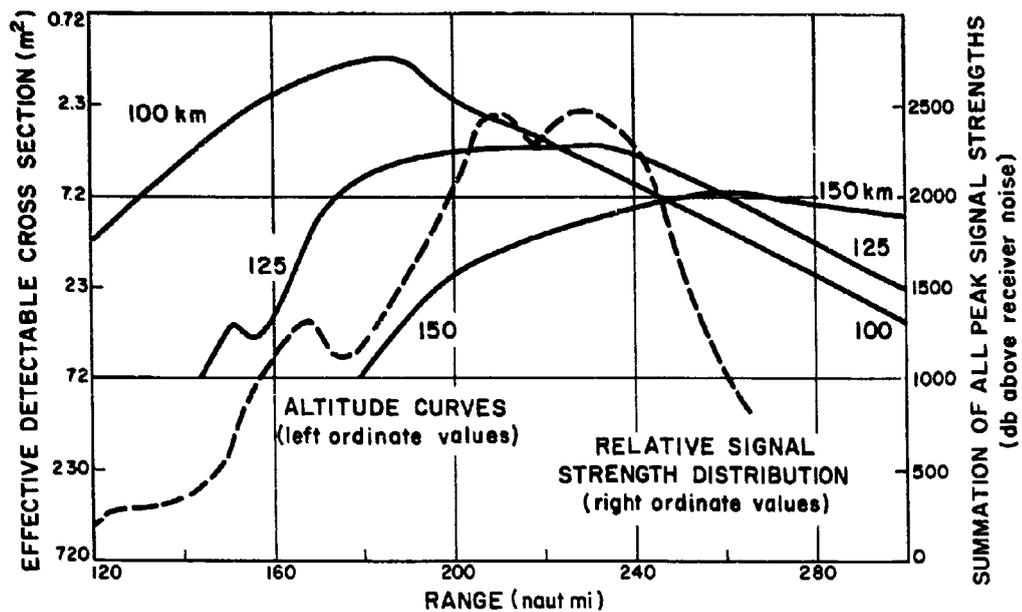
Figure 3.24 Signal strength distribution as a function of range overlayed on constant-altitude detection-capability curves.
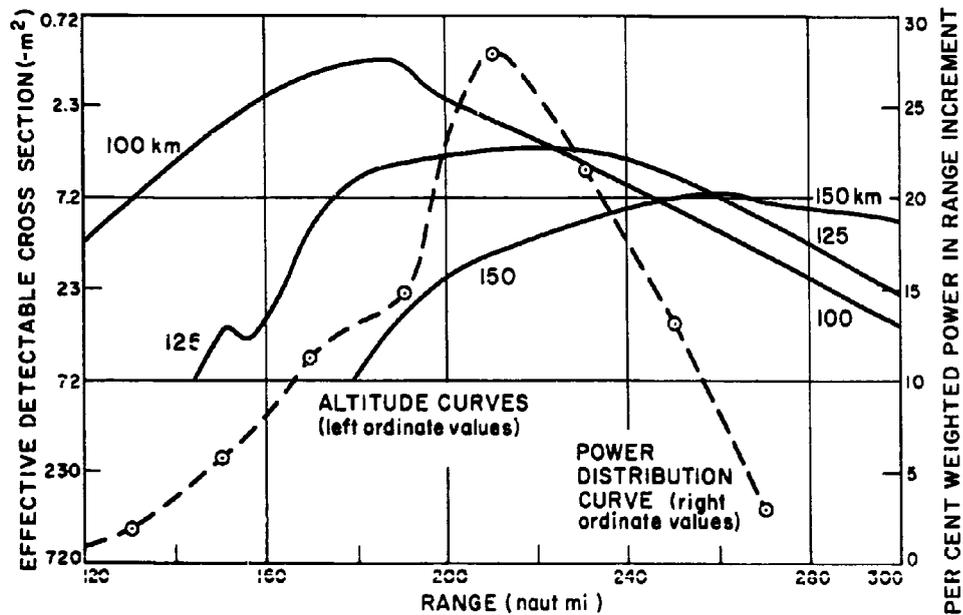
Figure 3.25 Power distribution as a function of range overlayed on constant-altitude detection-capability curves.

41

SECRET

3.7 PHASE COHERENCY OF RETURNS

Figure 3.26 shows a section of the photographic pulse-to-pulse recording. A total time of about one-half second is shown, each sweep encompassing 100 μsec of the 3.3-msec interpulse period, and located in the center of the area of returns. The data shown were taken from the 425-Mcps results on Shot Orange, at approximately H + 6 minutes. Two alternating video presentations appear, the narrower (in amplitude) being logarithmic video, for reference, and the other the phase-detected bipolar video. Coherency would be indicated by a sweep-to-sweep correspondence between the bipolar videos.

Only a cursory examination of this data was undertaken. In general, no phase coherency could be detected although occasionally a relatively slow phase shift was observed. This lack indicates a random distribution of velocity components of the scattering particles. The AMTI video presentation (pulse-to-pulse comparison of the bipolar) also indicated a non-coherency.

The examination of these data was insufficient to have detected any component of slow phase shift, and the effort required to obtain this information was not felt warranted. If desirable, the spectrum and distribution of velocity components of the backscattering elements could be derived from these data.

3.8 425-Mcps SHOT ORANGE, COMPARISON OF EARLY DATA WITH OTHER RESULTS

Most of the results given thus far have dealt with the 425-Mcps Shot Orange data from 6 to 21 minutes. In general, only qualitative statements can be made respecting the other data but some broad limitations can be derived. It can be seen from Figure 3.13 that the peak signal strengths on the 425-Mcps Shot Orange remained relatively constant at about 92 db below one milliwatt, between 6 and 21 minutes after burst. This, coupled with the average, weighted range of approximately 220 miles shown in Figure 3.24, and the detection capability at that range for 125-km altitude, leads to an average effective reflecting cross section of 820 square meters.

3.8.1 Other Times, 425-Mcps Shot Orange. It is not practical to discuss the data observed prior to the field alignment since the altitude of the reflecting medium, and hence the gain of the antenna, is not clear. Further, the signals received during the turns must be discarded since, again, the gain patterns during the banking of the aircraft are not readily determined.

However, the lack of signals observed after the second turn (49 minutes), when the aircraft heading, and thus the gain patterns, was identical to that during the earlier period, indicates an apparent reflecting cross section of less than 13 m^2. Figure 3.27 shows the reduction in performance due to antenna pattern, which would be expected during the period of 26 to 45 minutes at each of three altitudes. In this case, the signals are so sporadic that only speculation is possible. Looking merely at the groups of returns, disregarding the times where no signal was received, it does appear that the decline noted above, corrected by the performance reduction, could have taken place as a relatively smooth function of time.

3.8.2 425 Mcps, Shot Teak. Figure 3.28 depicts the results obtained on 425 Mcps for Shot Teak in a manner similar to Figure 3.13 of Shot Orange data. Again, no clear comparison can be made and only rough outer bounds can be determined.

The apparent great difference in signal strengths during the first 6 minutes could be due to the antenna gain patterns.

Shot Orange was detonated at a lower altitude and was subject to less thermodynamic rise. Therefore, the ionization sources were always located at a lower altitude than on Shot Teak. The antenna gain was higher for these lower altitudes and the signal strengths, consequently greater. After H + 6 minutes, when the reflecting medium has become field-aligned, presumably, the altitudes of ionization are comparable. The detection capabilities, including gain patterns and ranges, are essentially similar within 2 or 3 db, but the results are quite unlike. During the first 25 minutes, the Shot Teak data generally fall 10 or more db below

42
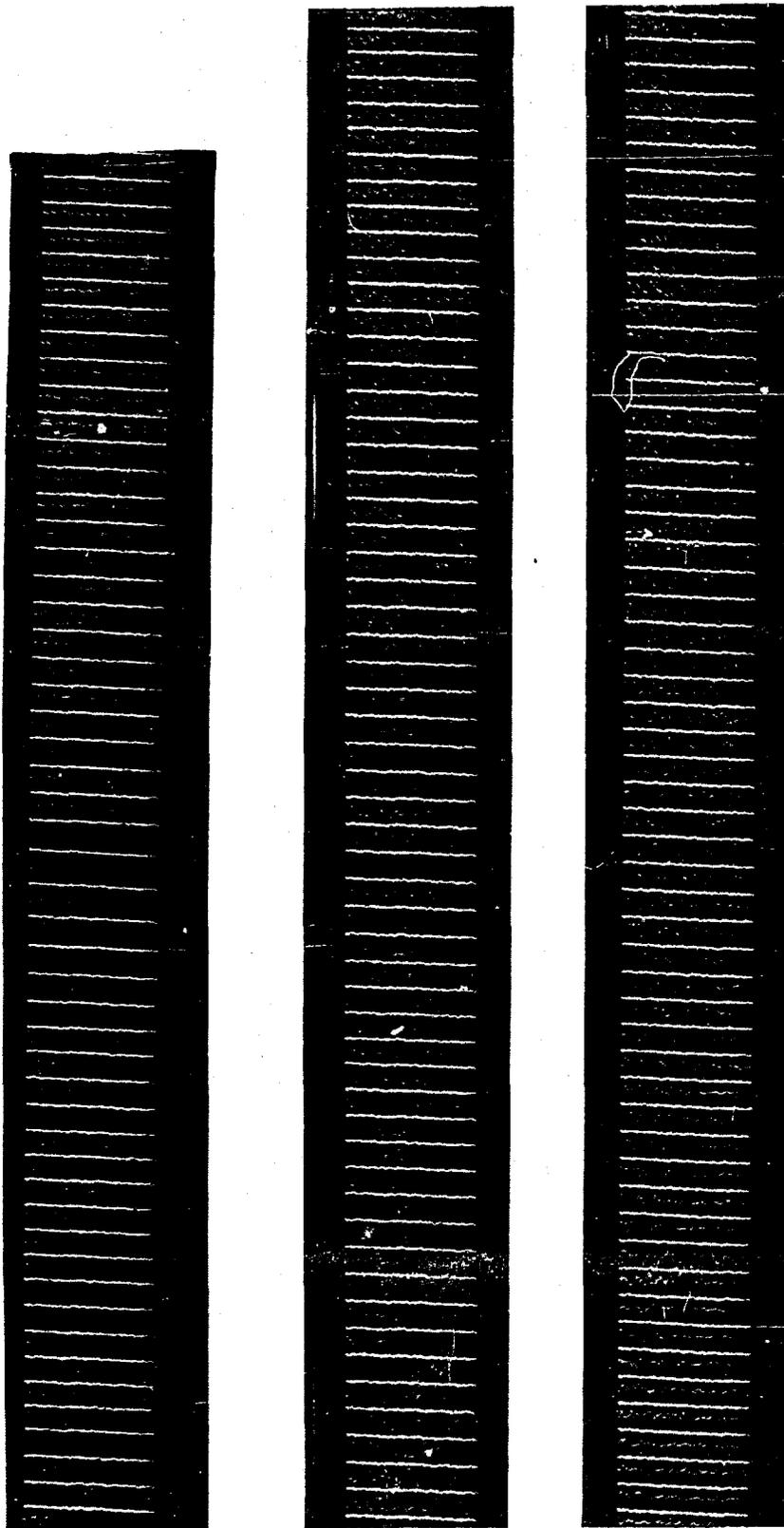
Figure 3.26 Pulse-to-pulse A-scan photographs.
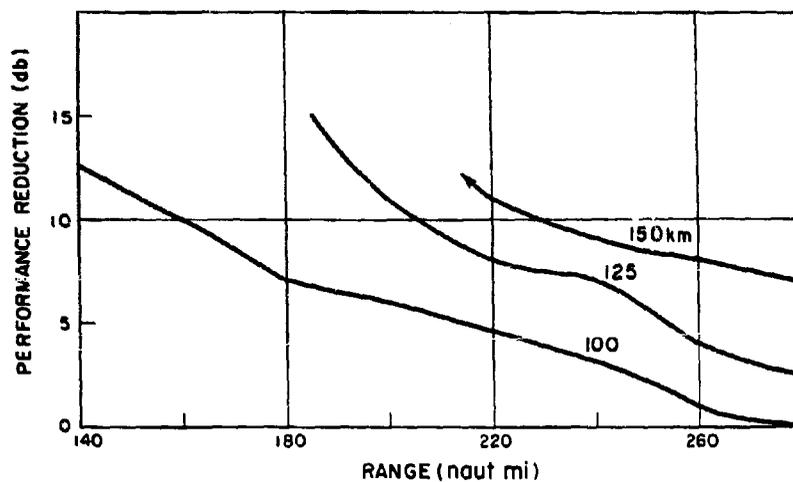
Figure 3.27 Expected reduction in performance from 425-Mcps radar following turn from 090 degrees M to 250 degrees M.
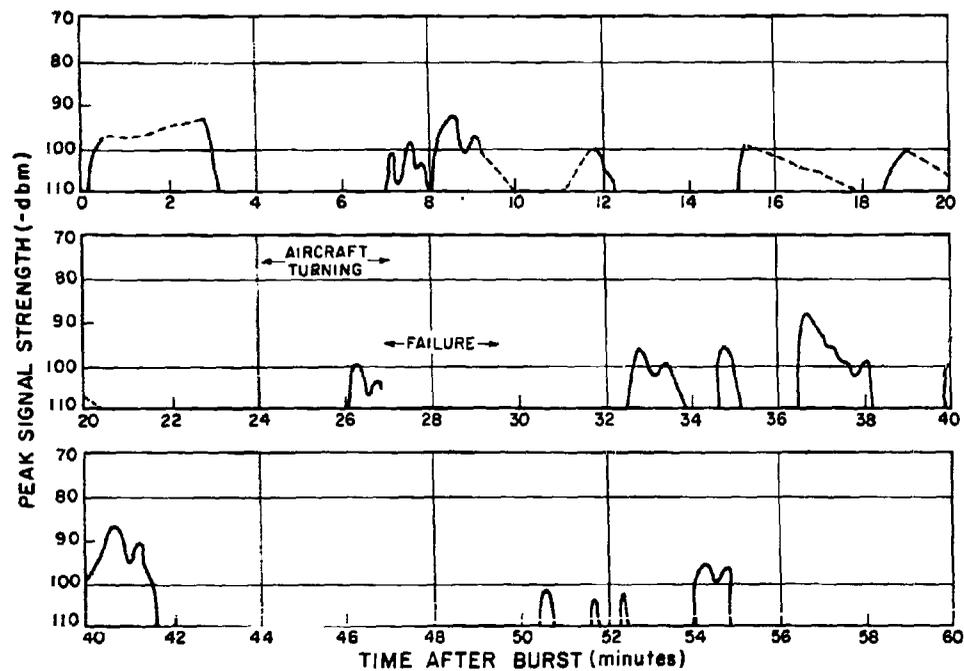
Figure 3.28 Most-intense signal strength versus time, 425 Mcps, Shot Teak.

44

SECRET
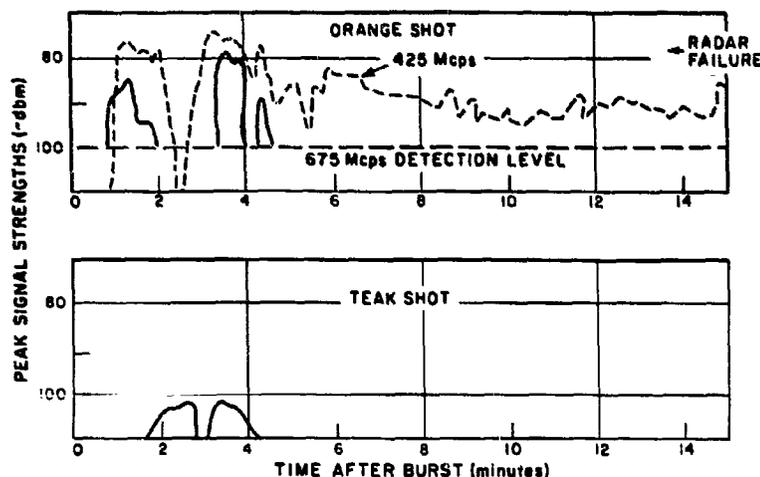
Figure 3.29 Most-intense signal strengths versus time, 675 Mcps.

the Shot Orange data. However, after 25 minutes, the Shot Teak results seem to indicate a stronger level of signals, even though the direct comparison must consider the variation in performance (for these times, the Teak detection capabilities exceed those on Orange by approximately the amounts shown in Figure 3.27).

3.8.3 675 Mcps. Figure 3.29 indicates the peak signal strengths observed at 675 Mcps on both shots, with the curve of Figure 3.13, indicated by a dashed line. Considering only the
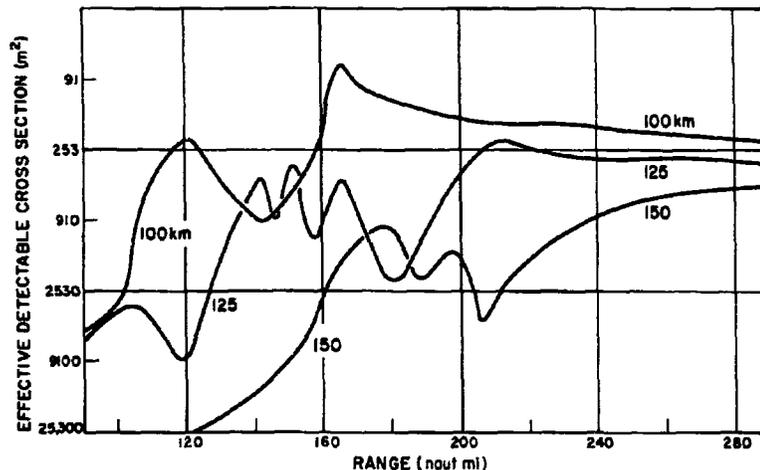
Figure 3.30 Detection capability as a function of range and altitude, 675 Mcps, Shot Orange.

Shot Orange data, the returns prior to H + 5 minutes correlate quite well in time but cannot be properly compared in amplitude. Again, the variation in detection capability with the height of the reflecting medium is indeterminate.

During the ensuing period of field-aligned ionization, the 675-Mcps radar detected no signals, although the altitudes of returns would be expected to be similar. The detection capability of this system is shown in Figure 3.30, taking into account the reduced sensitivity of the

45

SECRET

receiver due to malfunction. If the 125-km curve, from 200 miles out, is used as a basis for comparison, the average cross section capable of being detected was about 253 m^2. On the other hand, the 425-Mcps data for the same period indicated an apparent effective cross section of approximately 820 m^2. Thus the difference, of at least 5 db, can be attributed to a frequency dependence of reflection. It should be relatively safe, therefore, to conclude that the auroral back-scattering cross section is proportional to at least the two-and-a-half power of the wavelength, in the UHF radar band.

Chapter 4
SECONDARY EXPERIMENTS

4.1 ATTENUATION MEASUREMENTS AT 225 Mcps

4.1.1 Procedure.
Signals transmitted by the 225-Mcps series of rockets, of Sandia Corporation's Project 32.3, were to be received by a station aboard an aircraft at 8,000-foot altitude (see Figures 3.3 and 3.4). A standard AT-256/ARC antenna (dipole) mounted on top of the fuselage fed signals to a single-stage, grounded-grid amplifier (see Figure 4.1). The amplified signal was double-converted to 11 Mcps, detected, integrated and applied to a stylus-paper recorder. The characteristics were: frequency, 221 to 225 Mcps; noise figure, 2 db; bandwidth, 15 kcps.

At the programmed time of launch of the missiles carrying the transmitters, the receiver was tuned over the band of possible frequencies until a signal was obtained. Then the equipment was left untouched and the signal was recorded as long as the transmitter remained airborne.

4.1.2 Results, Shot Teak.
At H minus 10 seconds, signals on 224 Mcps were picked up at a strength of 18 db above the receiver noise level. The signal disappeared within one second after burst time. The recovery time of the signal is not known except that the loss exceeded two seconds since malfunction prevented observation of the recovery. At H + 2.75 minutes, the signal was present again with approximately the original magnitude. The phrase, "disappeared within one second," is due merely to the inaccuracy of the time scale and does not necessarily imply other than immediate loss of signal.

4.1.3 Results, Shot Orange.
At H − 1.17 minutes, a signal level of 19 db above receiver noise was attained on a frequency of 222 Mcps. This level remained almost constant until it disappeared within one second after burst time. The strengths are shown in Figure 4.2. At H + 0.50 minutes, the signal rose sharply out of noise to 19 db above the receiver noise. At H + 0.92 minutes, it again disappeared. From H + 1.28 to 15.0 minutes, a signal was present above the receiver saturation level (21 db above noise). This signal (not shown in Figure 4.2) is not believed to have originated from the missile transmitter, and no explanation of its existence has been determined.

4.1.4 Discussion of 225-Mcps Data.
Little can be determined from the data on Shot Teak. An apparent attenuation of something greater than 18 db occurred almost immediately following the detonation. The Sandia-received signals at the USS Belgrove, approximately 30 miles from Johnston Island in the same direction as our aircraft station, indicated an attenuation in excess of this level for a period exceeding 30 seconds, so no discrepancy is noted.

On Shot Orange, no 222-Mcps signals were recorded on the Belgrove. The other frequencies recorded there were transmitted from different trajectories, thus no valid comparison can be made without accurate path information. On Johnston Island, Sandia recorded approximate attenuations of 40 db or greater up to H + 0.42 minutes with something approaching an exponential fall to zero attenuation at about 50 seconds. The data of Paragraph 4.1.3 seem in reasonably close agreement; a more detailed analysis of the geometry and trajectories might yield a better picture of this correlation. The saturated signals observed after one minute do not seem to be of any significance.

47

SECRET

4.2 NOISE MEASUREMENT AT 31 Mcps

4.2.1 Procedure. A three-element Yagi antenna directed vertically upward was located on Oahu approximately 1,000 km from the burst. This antenna had a beamwidth of approximately 50 degrees. The RF from the antenna was amplified at 31 Mcps (bandwidth, 4 Mcps), mixed with 70 Mcps from a tunable oscillator, and amplified at 40 Mcps. The bandwidth of the final amplifier was about 500 kcps. An integration network, with a time constant of approxi-
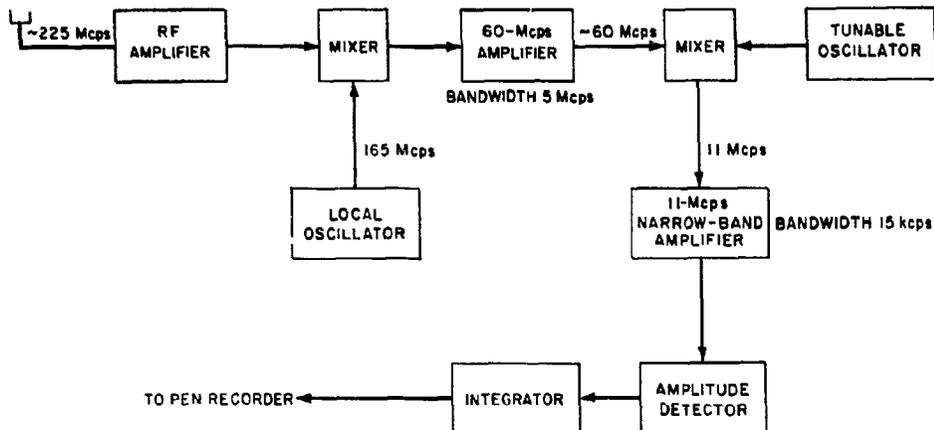
Figure 4.1 225-Mcps receiver.

mately 0.01 sec, fed signals directly to the pen recorder (response to 100 cps). The receiver noise figure was less than one db. Cosmic noise was recorded continuously over comparatively long periods of time to establish the ambient levels during the tests.

4.2.2 Results. The results from both shots are presented in Figure 4.3. On Shot Teak, the ambient noise level was approximately 7 db above thermal noise. An immediate increase
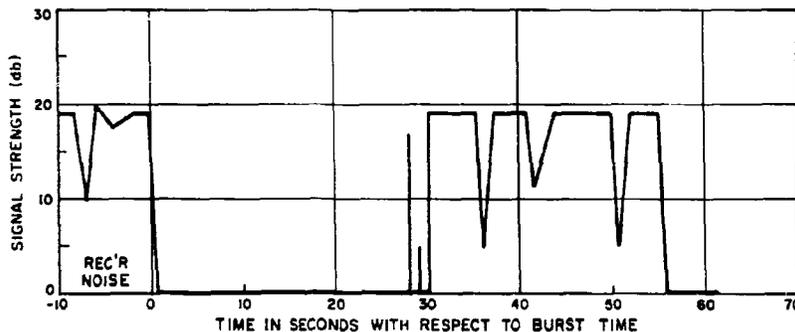
Figure 4.2 225-Mcps rocket-borne beacon signals, Shot Orange.

in noise of approximately 2.5 db was observed, falling through ambient in less than one second, thence indicating a lower noise for approximately five more seconds when recovery was completed.

On Shot Orange, the ambient level was about 8.5 db above thermal noise. At burst time, the noise level rose to saturation (increase of greater than 2.5 db) and remained there for slightly more than one second. This was followed by a drop to 1.5 db below ambient, remain-

48

SECRET

ing at this level for about 20 minutes and recovering comparatively sharply to the normal ambient level.

4.2.3 Discussion. The increase in noise level appears to be real in both cases. The fact that it was not observed by the various Riometers[1] of the Stanford Research Institute (SRI) does not seem to be incompatible in view of the longer integration times of the Riometers. It appears therefore, that this increase must be explained by either the radiation of electromagnetic energy from the detonation processes or by reflections from the ionized stratum of
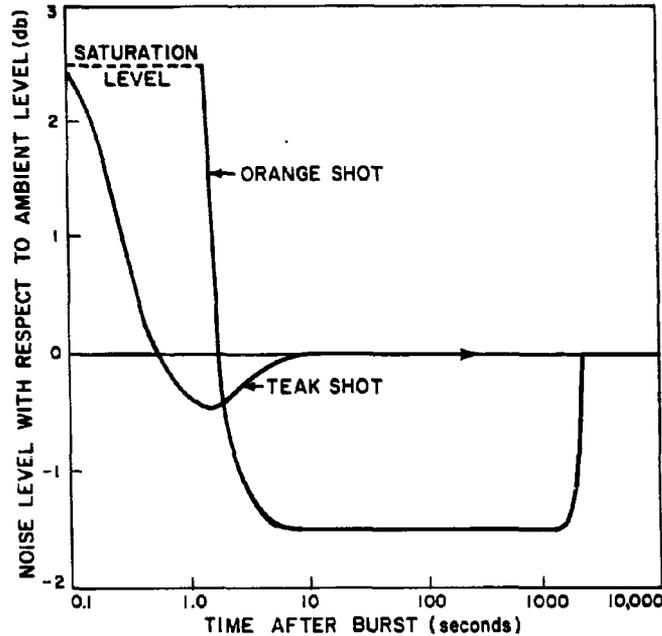
Figure 4.3 31-Mcps noise monitoring results.

an interference source well beyond the line-of-sight. In view of the probable attenuations at this frequency, which would mitigate the effect of such a reflection, the former reasoning would seem more plausible.

There exists somewhat more doubt as to the validity of the 20-minute period of attenuation. The conflict with the SRI Riometer data is large and no readily apparent instrumental incongruity has been found. The Lincoln and SRI units on Oahu were observing approximately the same area and with no great difference in performances. The only real difference was in operating frequency (28 versus 31 Mcps). The authors are not able to explain the discrepancy although at least two possibilities exist: (1) an undetected malfunction or change in receiver noise level could have occurred in one or the other equipments; (2) interference from a distant source might have contributed to the ambient level before the shot (and after H + 20 minutes) with its reflection subjected to absorption following the burst.

---

[1] Cosmic-noise monitoring equipments of Project 6.11. The SRI equipment, with integration times on the order of seconds, did not observe any increase in noise level above the preshot ambient.

49

SECRET

4.3 NOISE MEASUREMENT AT 113 Mcps

4.3.1 Procedure. RF signals at 113 Mcps were received by the standard aircraft VOR antenna and amplified by a grounded-grid amplifier with 3 Mcps bandwidth. The input to the RF amplifier was alternated mechanically with the signals of a precision noise source with variable output. The amplified signals were then mixed down to 30 Mcps, further amplified and narrowed to a bandwidth of 500 kcps. The output of this amplifier was used to drive a stylus-paper recorder, a voltmeter, and an audio amplifier and speaker. The input from the noise source was adjusted to match the noise level observed by the antenna, and the values of noise required to achieve this balance were then read from the calibrated noise generator and recorded as a function of time.
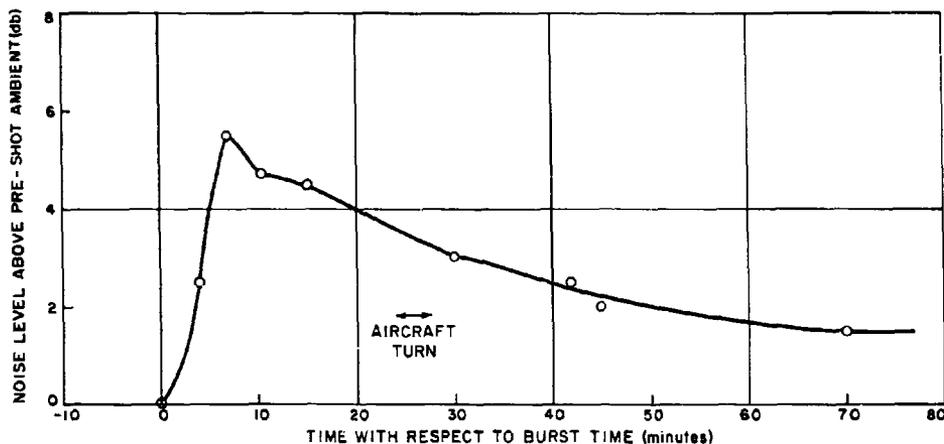
Figure 4.4 113-Mcps, Shot Teak noise monitor results.

4.3.2 Results. The measurements during the Teak event are plotted in Figure 4.4. The preshot ambient level indicated was approximately 2.5 db above thermal noise. No effect was observed until three minutes after the burst, at which time, the noise level increased to a peak, at H + 7 minutes, of 5.5 db above ambient. The level then slowly decreased to a value of 1.5 db above the pre-shot ambient at H + 70 minutes, and remained at that level until H + 191 minutes, at which time the equipment was secured.

No change in noise level was observed on Shot Orange.

4.3.3 Discussion. If the effect noted on Shot Teak is real, there is some conflict with the measurements of other projects although none duplicated the Lincoln measurements. Even with the uncertainties of the antenna pattern, [2] it is probable that some consequential effect would have been observed during or following the turn indicated in Figure 4.4, had the source of the increased noise been directional in nature. The 1.5 db above ambient noise level be-

---

[2] The patterns of the VOR antenna are not known but, from its location (in the nose cone of the aircraft), it is assumed to be somewhat directional forward. The use of an antenna with unknown characteristics was necessitated by the fact that this was the only one available in the allotted time for preparation. The relative azimuths of air zero, with respect to the aircraft heading, as a function of time after burst, were as follows, Shot Teak, 0 to 24 minutes, 335 degrees; 27 to 58 minutes, 150 degrees. Shot Orange, 0 to 21 minutes, 155 degrees; 24 to 48 minutes, 355 degrees.

50

SECRET

yond H + 70 minutes may be attributable to an increase in either receiver or local noise (such as ignition noise from the engines caused by a change in engine speeds).

It is possible, therefore, that the increases noted were due to the immediate environment rather than to the effects of the detonation; however, the increase in noise level shortly after the shot, which was never experienced in any test flights, might lead one to believe that it was due to the detonation.

4.4 UHF NOISE MEASUREMENTS

4.4.1 Procedure. Receivers on frequencies of 425, 450 and 675 Mcps were carried in the aircraft for other experiments. These were connected to, respectively: a rotating array with 9 degree beam; a fixed dipole on a reflector; and a rotating array with 6 degree beam. In order to monitor any possible generation of comparatively long-time intense noise, separate receiver outputs were integrated and fed into a stylus-paper recorder. It is important to note that the instrumentation was such that noise, to be detectable, would have to exceed thermal noise by about 6 db and, in the case of the rotating arrays, would have needed sufficient duration to allow the antenna to scan past the source (scan rate, 6 rpm).

4.4.2 Results. No change in noise level was observed.

4.5 OTHER MEASUREMENTS

This chapter has dealt with all experiments conducted or attempted except the radar tests on frequencies of 425 and 675 Mcps. No data, either positive or negative, was collected from the 9,375-Mcps radar or from the experiments designed to passively monitor the rocket-borne transmissions at 1,500 Mcps (Project 32.3) and at 450 and 2,900 Mcps (Project 6.12). Because these experiments can in no way contribute, they have not been further discussed.

51

SECRET

Chapter 5
CONCLUSIONS

The results of this experiment can be summarized by the following conclusions regarding UHF radar effects. An immediate period of no reflected signal, presumably due to electromagnetic absorption, followed the detonations. This period was longer for the lower burst. Strong reflection occurred after the period of absorption, indicating electron densities in excess of approximately 10^9 electrons per cubic centimeter. The ionized region slowly diffused and became aligned with the earth's magnetic field. After a few minutes, this field-aligned ionization resembled auroras in every respect observed. Such a comparison includes considerations of altitude, aspect sensitivity and apparent east-west motion. Because of the aspect sensitivity of auroral returns, the region of sky from which these returns could have been observed, by appropriately placed radars, was no doubt vastly greater than the 50 × 150-mile region where they were detected in this experiment.

Although effects of significant proportions could have occurred with regard to refractive properties other than the reflections, no measurements were possible with the instrumentation available. Such effects could include either a bending of the propagated beam, without loss of definition, or a loss of energy and definition through scattering.

The possibility of noise generation in the UHF band, by synchrotron radiation of relativistic electrons trapped in the magnetic field, was considered. If this occurred, it was not of sufficient magnitude to be detected in this experiment. At these burst altitudes and frequencies, therefore, it is probably not an important effect.

Appendix
GENERAL FIGURES RELATING to PROJECT GEOMETRY
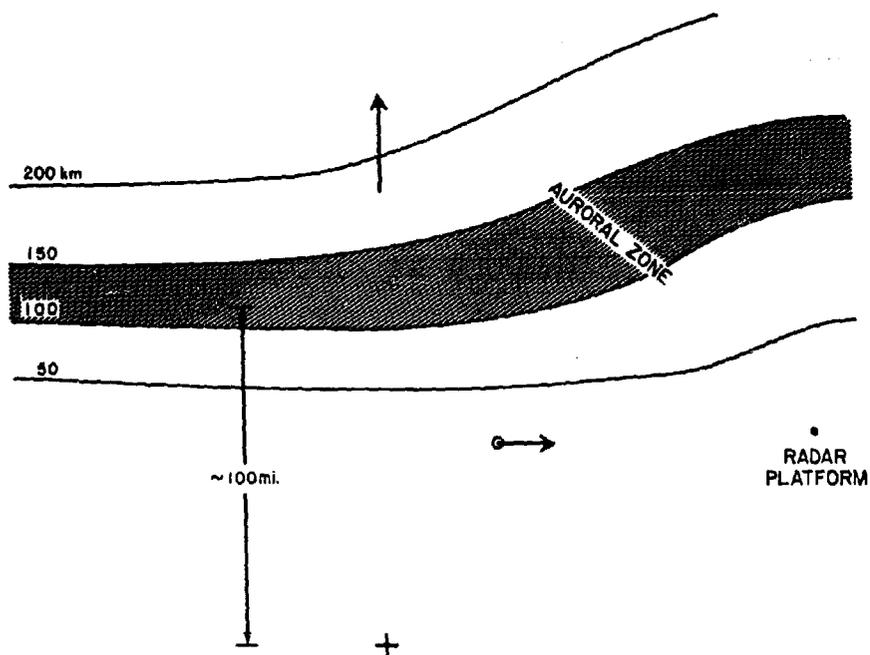
Figure A.1 Typical geometry of Project 6.13.
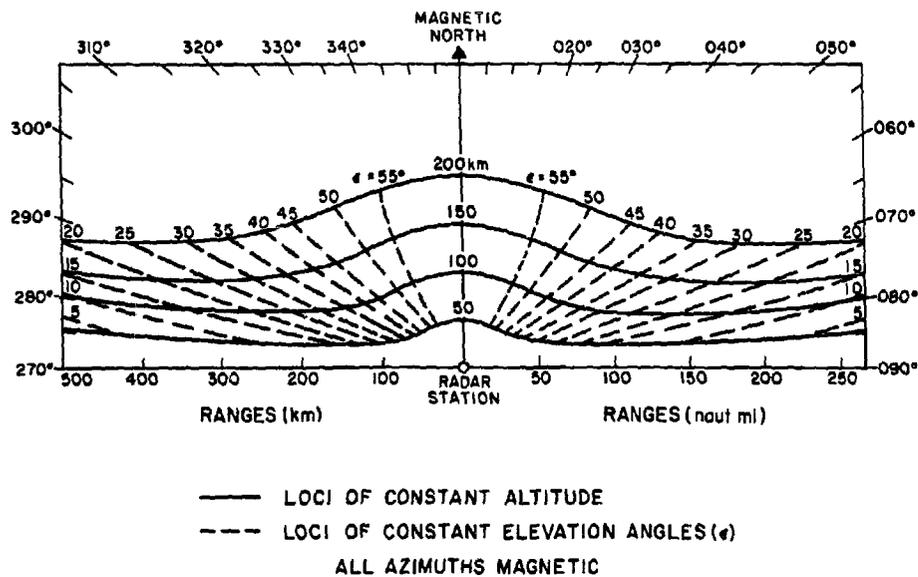
Figure A.2 Loci of perpendicularity for station at approximately
17 degrees N 170 degrees W.

54

REFERENCES

1. R. Meyerott; "Ultra-High Altitude Measurement Feasibility Study"; LMSD-2300; Lockheed Aircraft Corporation, Burbank, California.

2. H. L. Mayer; "Early History of High Altitude Nuclear Explosions"; Aeronutronics Systems, Inc., AFSWC-TR-57-16, 31 May 1957; Air Force Special Weapons Center, Albuquerque, New Mexico; Secret Restricted Data.

3. P. A. Caldwell, T. D. Hanscome, and W. E. Kunz; "Attenuation of High Frequency and Ultra High Frequency by Ionization Resulting from Nuclear Explosions"; Project 6.6, Operation Redwing, ITR—1346, July 1956; Naval Research Laboratory, Washington 25, D. C.; Secret Restricted Data.

4. N. C. Christofilos; UCRL COPD-58-2; University of California Radiation Laboratory, Livermore, California; Secret Restricted Data.

5. H. G. Booker, et al; "Interpretations of Radio Reflections from the Aurora"; Journal of Geophysical Research 60, 1 (1955).

6. T. R. Kaiser; "Radio Investigations of Aurorae and Related Phenomena"; paper presented at Symposium in Belfast, 1955 and recorded in "The Airglow and the Aurorae"; Editors, Armstrong and Dalgarno.

7. A. M. Peterson, et al; "Regularly-Observable Aspect-Sensitive Radio Reflections from Ionization Aligned with the Earth's Magnetic Field and Located Within the Ionospheric Layers at Middle Latitudes"; Journal of Geophysical Research 60, 4 (1955).

8. R. B. Dyce; "Auroral Echoes Observed North of the Auroral Zone on 51.9 Mcps/sec"; Journal of Geophysical Research, 60, 3 (1955).

9. S. J. Fricker, et al; "UHF Radar Observations of Aurora"; Journal of Geophysical Research 62, 4 (1957).

10. S. Chapman; "The Geometry of Radio Echoes from Aurorae"; Journal of Atmospheric and Terrestrial Physics 3, 1 (1952).

11. E. B. Giller, et al; "Effects of Nuclear Weapons in Space, a Test Concept"; AFSWC-TN-58-4; Air Force Special Weapons Center, Albuquerque, New Mexico; Secret Restricted Data.

12. "An Experimental Study of the Effects of the WV-2 Aircraft upon the Radiation Patterns of an Airborne UHF Radar"; Lockheed Aircraft Corporation Report 10989.

13. W. A. Cummings and J. C. Barnes; "An Antenna for Airborne Early Warning"; National Research Council of Canada, Report ERB-464.

14. D. H. Griffin and J. H. Lee; "Preliminary Handbook — Operating Instructions for IF Cancellation Receivers"; Massachusetts Institute of Technology, Lincoln Laboratory Group Report 45-31.

15. D. H. Griffin, et al; "The IF TACCAR AMTI System"; Massachusetts Institute of Technology, Lincoln Laboratory Group Report 45-28.

16. H. R. Reed and E. M. Russell; "Ultra High Frequency Propagation"; J. Wiley and Sons, Inc., New York, 1953.

DISTRIBUTION

Military Distribution Category 62

ARMY ACTIVITIES

1 Deputy Chief of Staff for Military Operations, D/A, Washington 25, D.C. ATTN: Dir. of SWAR
2 Chief of Research and Development, D/A, Washington 25, D.C. ATTN: Atomic Div.
3 Assistant Chief of Staff, Intelligence, D/A, Washington 25, D.C.
4 Chief of Engineers, D/A, Washington 25, D.C. ATTN: ENGNB
5 Chief of Engineers, D/A, Washington 25, D.C. ATTN: ENGTB
6- 7 Office, Chief of Ordnance, D/A, Washington 25, D.C. ATTN: ORDTN
8 Chief Signal Officer, D/A, Plans, Programs, and Ops. Div., Washington 25, D.C. ATTN: SIGOP-7A
9- 11 Commanding General, U.S. Continental Army Command, Ft. Monroe, Va.
12 Director of Special Weapons Development Office, Headquarters CONARC, Ft. Bliss, Tex. ATTN: Capt. Chester I. Peterson
13 President, U.S. Army Artillery Board, Ft. Sill, Okla.
14 President, U.S. Army Air Defense Board, Ft. Bliss, Tex.
15 President, U.S. Army Aviation Board, Ft. Rucker, Ala. ATTN: ATBG-DG
16 Commandant, U.S. Army Command & General Staff College, Ft. Leavenworth, Kansas. ATTN: ARCHIVES
17 Commandant, U.S. Army Air Defense School, Ft. Bliss, Tex. ATTN: Command & Staff Dept.
18 Commandant, U.S. Army Armored School, Ft. Knox, Ky.
19 Commandant, U.S. Army Artillery and Missile School, Ft. Sill, Okla. ATTN: Combat Development Department
20 Commandant, U.S. Army Aviation School, Ft. Rucker, Ala.
21 Commandant, U.S. Army Infantry School, Ft. Benning, Ga. ATTN: C.D.S.
22 Commanding General, Chemical Corps Training Comd., Ft. McClellan, Ala.
23 Commandant, USA Signal School, Ft. Monmouth, N.J.
24 Commanding Officer, Army Medical Research Lab., Ft. Knox, Ky.
25 Commanding General, U.S. Army Chemical Corps, Research and Development Comd., Washington 25, D.C.
26 Commanding Officer, Chemical Warfare Lab., Army Chemical Center, Md. ATTN: Tech. Library
27 Commanding Officer, Diamond Ord. Fuze Labs., Washington 25, D.C. ATTN: Chief, Nuclear Vulnerability Br. (230)
28 Commanding General, Aberdeen Proving Grounds, Md. ATTN: Director, Ballistics Research Laboratory
29- 30 Commanding General, U.S. Army Ord. Missile Command, Redstone Arsenal, Ala.
31 Commander, Army Rocket and Guided Missile Agency, Redstone Arsenal, Ala. ATTN: Tech Library
32 Commanding General, White Sands Proving Ground, Las Cruces, N. Mex. ATTN: ORDBS-OM
33 Commander, Army Ballistic Missile Agency, Redstone Arsenal, Ala. ATTN: ORDAB-HT
34 Commanding General, Ordnance Ammunition Command, Joliet, Ill.
35 Commanding Officer, USA Signal R&D Laboratory, Ft. Monmouth, N.J.
36 Commanding General, U.S. Army Electronic Proving Ground, Ft. Huachuca, Ariz. ATTN: Tech. Library
37 Commanding General, USA Combat Surveillance Agency, 1124 N. Highland St., Arlington, Va.
38 Commanding Officer, USA Signal R&D Laboratory, Ft. Monmouth, N.J. ATTN: Tech. Doc. Ctr., Evans Area
39 Director, Operations Research Office, Johns Hopkins University, 6935 Arlington Rd., Bethesda 14, Md.
40 Commanding General, U.S. ORD Special Weapons-Ammunition Command, Dover, N.J.

NAVY ACTIVITIES

41 Chief of Naval Operations, D/N, Washington 25, D.C. ATTN: OP-03EG
42 Chief of Naval Operations, D/N, Washington 25, D.C. ATTN: OP-75
43 Chief of Naval Operations, D/N, Washington 25, D.C. ATTN: OP-92201
44- 45 Chief of Naval Research, D/N, Washington 25, D.C. ATTN: Code 811
46- 48 Chief, Bureau of Naval Weapons, D/N, Washington 25, D.C. ATTN: DLI-3
49 Chief, Bureau of Ordnance, D/N, Washington 25, D.C.
50 Chief, Bureau of Ships, D/N, Washington 25, D.C. ATTN: Code 423
51 Director, U.S. Naval Research Laboratory, Washington 25, D.C. ATTN: Mrs. Katherine H. Cass
52- 53 Commander, U.S. Naval Ordnance Laboratory, White Oak, Silver Spring 19, Md.
54 Commanding Officer and Director, Navy Electronics Laboratory, San Diego 52, Calif.
55 Commanding Officer, U.S. Naval Mine Defense Lab., Panama City, Fla.
56 Commanding Officer, U.S. Naval Radiological Defense Laboratory, San Francisco, Calif. ATTN: Tech. Info. Div.
57 Commanding Officer, U.S. Naval Schools Command, U.S. Naval Station, Treasure Island, San Francisco, Calif.
58 Superintendent, U.S. Naval Postgraduate School, Monterey, Calif.
59 Commanding Officer, Air Development Squadron 5, VX-5, China Lake, Calif.
60 Commandant, U.S. Marine Corps, Washington 25, D.C. ATTN: Code AO3H
61 Director, Marine Corps Landing Force, Development Center, MCB, Quantico, Va.
62 Commanding Officer, U.S. Naval CIC School, U.S. Naval Air Station, Glynco, Brunswick, Ga.

AIR FORCE ACTIVITIES

63 Deputy Chief of Staff, Development, HQ. USAF, Washington 25, D.C. ATTN: AFDRD
64- 65 Air Force Intelligence Center, HQ. USAF, ACS/I (AFCIN-3V1) Washington 25, D.C.
66 Director of Research and Development, DCS/D, HQ. USAF, Washington 25, D.C. ATTN: Guidance and Weapons Div.
67 Commander, Tactical Air Command, Langley AFB, Va. ATTN: Doc. Security Branch
68 Commander, Air Defense Command, Ent AFB, Colorado. ATTN: Assistant for Atomic Energy, ADLDC-A
69 Commander, HQ. Air Research and Development Command, Andrews AFB, Washington 25, D.C. ATTN: RDRWA
70 Commander, Air Force Ballistic Missile Div. HQ. ARDC, Air Force Unit Post Office, Los Angeles 45, Calif. ATTN: WDSOT
71 Commander, Second Air Force, Barksdale AFB, La. ATTN: Operations Analysis Office
72 Commander, Eighth Air Force, Westover AFB, Mass. ATTN: Operations Analysis Office
73 Commander, Fifteenth Air Force, March AFB, Calif. ATTN: Operations Analysis Office
74 Commander, Air Proving Ground Center, Eglin AFB, Fla. ATTN: PGTRIL
75- 76 Commander, AF Cambridge Research Center, L. G. Hanscom Field, Bedford, Mass. ATTN: CRQST-2
77- 81 Commander, Air Force Special Weapons Center, Kirtland AFB, Albuquerque, N. Mex. ATTN: Tech. Info. & Intel. Div.

SECRET

SECRET

SECRET

20 February 2004

BDQ (505) 846-0847

To: Larry Downing, DTIC

Subject: Re-Review of DNA reports

Here is the fifth increment of the results of the re-review project:

   See Attached List

We will send more as they are reviewed.

Brenda M. Steward
COTR,
Defense Threat Reduction Information
Analysis Center (DTRIAC)

REPORT NO.	AD NO.	CLASS.	DISTRIBUTION
WT 1659	360459	Unc.	A
DNA 5170F	C022641	Unc.	D, Admin Operational
DASA 1456-2	826837	Unc.	A
DASA 1394	340878	Unc.	A
DASA 1329	292079	Unc.	A
DASIAC-B-SP-72-3	525010	Unc.	C, Admin Operational
DASIAC-B-SP-74-1	531258	Unc.	C, Admin Operational
DASIAC-B-SP-72-2	525009	Unc.	C, Admin Operational
DASIAC-SR-126	518928	Unc.	C, Admin Operational
DASA 1277-1	465914	Unc.	C, Critical Technology
DASA 1226	323067	Unc.	C, Test and Evaluation
DASA 1476	352148	Unc.	C, Test and Evaluation
POR 6728	528917	**CFRD**	C, Test and Evaluation
DASA 1477	352146	Unc.	C, Test and Evaluation
DASA 1493	355872	Unc.	C, Test and Evaluation
POR 6660	527793	**CFRD**	C, Test and Evaluation
DNA 5181F	C026283	Unc.	C, Test and Evaluation
DASA 1586	359301	Unc.	C, Test and Evaluation
DASA 1601	363360	Unc.	C, Test and Evaluation
DASA 1668	365521	Unc.	C, Test and Evaluation
DASA 1565-1	356449	Unc.	C, Test and Evaluation